5-2016

The MH-2 Core from Project Hotspot: Description, Geologic Interpretation, and Significance to Geothermal Exploration in the Western Snake River Plain, Idaho

Jerome A. Varriale
Utah State University

THE MH-2 CORE FROM PROJECT HOTSPOT: DESCRIPTION, GEOLOGIC INTERPRETATION, AND SIGNIFICANCE TO GEOTHERMAL EXPLORATION IN THE WESTERN SNAKE RIVER PLAIN, IDAHO

by

Jerome A. Varriale

A thesis submitted in partial fulfillment
of the requirements for the degree

of

MASTER OF SCIENCE

in

Geology

Approved:

Dr. James P. Evans Major Professor	Dr. John W. Shervais Committee Member
Dr. Kelly K. Bradbury Committee Member	Dr. Mark McLellan Vice President for Research and Dean of the School of Graduate Studies

UTAH STATE UNIVERSITY
Logan, Utah

2016

ABSTRACT

THE MH-2 CORE FROM PROJECT HOTSPOT: DESCRIPTION, GEOLOGIC INTERPRETATION, AND SIGNIFICANCE TO GEOTHERMAL EXPLORATION IN THE WESTERN SNAKE RIVER PLAIN, IDAHO

by

Jerome A. Varriale, Master of Science

Utah State University, 2015

Major Professor: Dr. James P. Evans
Department: Geology

The MH-2 science drill hole, on Mountain Home Air Force Base, Idaho, was drilled in 2012 to a total depth 1821 m as part of Project Hotspot. It encountered flowing artesian thermal water at 1,745 m below ground surface. This signature of a potential blind high temperature geothermal resource indicates that further analyses are needed to characterize the resource. Whole rock core was recovered to a total depth of 1821 m below ground surface and a suite of wireline logs collected. In this thesis I describe the lithologies represented in the core, correlate these lithologies to outcrop analogs, and identify and characterize petrophysical properties observable within the wireline logs, which represent fine-scale variations in stratigraphy, composition and/or alteration.

The lithologies in the core are a series of basalts, brecciated and altered basalt, basaltic sands, carbonate-rich muds, and siliciclastic sediments. Basalt flows with evidence of increasing influence of an aqueous environment with time typify

the lower half of core, whereas the upper half represents a period of diminished volcanism, lacustrine depositional environment, and a catastrophic water overflow event. The top of the core represents a resurgence of basaltic volcanism in the area. An overprint of brecciation at depth, fracturing, and secondary mineralization records the history of the geothermal system.

All the elements of a relatively shallow and potentially energy generating geothermal resource are present at the MH-2 well location. These new data from the MH-2 borehole contributes to evaluating a parallel geothermal risk assessment of the Snake River Plain. Play fairway analysis was implemented for perhaps the first time in a geothermal regime. The Snake River Plain was divided up into three distinct play types; the area surrounding the Mountain Home Air Force Base was systematically identified as prospective. A region where sedimentary and altered rocks may create a seal, and blind faults create porosity in deep basalts.

(89 pages)

PUBLIC ABSTRACT

THE MH-2 CORE FROM PROJECT HOTSPOT: DESCRIPTION, GEOLOGIC INTERPRETATION, AND SIGNIFICANCE TO GEOTHERMAL EXPLORATION IN THE WESTERN SNAKE RIVER PLAIN, IDAHO

Jerome A. Varriale

Harnessing the earth's natural heat generation as an energy resource has seen increased interest in recent history. While geothermal energy is a sustainable, low-carbon emitting, and viable source of energy in certain regions, large upfront risks, including costs of exploration and deep well drilling, have kept private sector investment at bay. Lowering the risks to capital investment that are inherent to subsurface exploration can help to assuage investors and bring this well-known energy-generating technology to the masses.

A blind potential geothermal system was encountered while drilling the MH-2 science drill hole, on Mountain Home Air Force Base, Idaho. The MH-2 hole was cored from 163 m to a total depth of 1,821 m, including through the thermal zone at 1,745 m, where flowing artesian thermal water was encountered. Characterizing this system can help to predict where similar systems may occur, to be targeted for future geothermal exploration projects. This work characterizes the geothermal system on the most fundamental level by describing, in detail, the lithologies present in the MH-2 core. These lithologies indicate the presence of a geothermal

fluid reservoir and seal, the elements required for a viable geothermal resource, and at a relatively shallow depth.

A parallel geothermal exploration project in southern Idaho has implemented petroleum subsurface exploration techniques to test the predictive ability to identify resources in a geothermal regime. The results show that this process has systematically identified the area surrounding the MH-2 site as prospective, and indicates the possibility of lowering risk in subsurface evaluation in geothermal exploration and production.

ACKNOWLEDGMENTS

I would first like to thank Dr. James Evans for taking me on under complicated circumstances, and giving me a new opportunity to work on a challenging and rewarding project aligned with my strengths, personal interests, and career goals. His advisement has greatly impacted the course of my professional career and personal life in an amazingly positive way. I owe a great deal of gratitude to him, far beyond this short paragraph, and I will never forget his generosity and understanding during a very difficult transition in my life.

Thank you to my committee members: Dr. John Shervais, the primary investigator of Project Hotspot, the main project from which this work is based on, for allowing me unfettered access to the MH-2 core, all associated data, and his career-long knowledge base of the study site and greater Snake River Plain. I would also like to thank him for giving me the opportunity and great responsibility of managing the mapping database for the geothermal exploration project. Thank you to Dr. Kelly Bradbury for your support and direction with the XRD and thin section analysis portion of this work, as well as your insight into core logging.

Thank you to my family, friends, and colleagues for all of your support and guidance through this process. Most deserving of my gratitude, my wife, Maria, thank you for your unending support and love! And, thank you to my daughter, Evelyn Ida, for inspiring a happiness I never knew existed, and for providing a higher level of motivation to be the best man I can be.

Parts of this research were supported by Department of Energy award DE-EE0003733 and the MH-2 core samples provided by Project Hotspot, Department of Energy award DE-EE002848.

CONTENTS

LIST OF TABLES AND PLATES

LIST OF FIGURES

INTRODUCTION

In 2012 the MH-2 scientific drill hole, on the Mountain Home Air Force Base (MHAFB), Mountain Home, Idaho, in the Western Snake River Plain geologic province (Figure 1), was drilled as part of a Utah State University led 3-hole research project, that drilled in the track of the Yellowstone Hotspot, Project Hotspot (Shervais et al., 2013, 2014). The MH-2 hole, drilled to 1821. 5 m below ground surface, encountered artesian high-temperature geothermal water with a down-hole temperature of at least 140 °C (Shervais et al., 2013; Freeman, 2013; Atkinson, 2015). A total of 1,658 m (from 163.1 – 1,821.5 m below ground surface) of whole rock core were recovered from the borehole and a full suite of wireline logs from 1,165 to 1,675 m bgs were collected, providing the opportunity to characterize the lithologic, stratigraphic, structural, geochemical, and geomechanical elements present at this new and potentially important site for future geothermal resource evaluation and the surrounding area.

Kessler (2014) used borehole breakout data to characterize the *in-situ* stress, and related geomechanical rock properties and fracture densities of the lower 548 m of core to characterize the spatial distribution of reservoir and seal of the geothermal system. He identified a maximum horizontal stress striking ~ N 45° E, ~90° away from the expected stress state, and theorized the presence of a proximal intrabasinal stepover fault to explain this orientation. Freeman (2013) characterized the geochemistry of the geothermal fluid as a Na-sulfate type water, and determined that it is not meteoric in origin, using isotope analysis, which suggests that the water may be equilibrated with the geothermal system.

Atkinson (2015) analyzed fluid inclusions and stable isotopic compositions of samples of secondary mineralization in veins from the basalts 50 m above and below the thermal zone, to determine maximum temperatures of the geothermal fluid, based on fluid inclusions and mineralization properties. He determined that temperatures were at one time at least 260 °C, and possibly as hot as 370 °C (Atkinson, 2015).

This thesis characterizes the lithologies, textural properties and mineralogical compositions present in the MH-2 core. Each litho-stratigraphic interval represents the history of emplacement or deposition, stress related deformation, and secondary mineralization and porosity development. Integrating the results of this work with Kessler (2014), Freeman (2013), and Atkinson (2015) increases the knowledge base of the geology of the Western Snake River Plain, and adds insight into the potential for geothermal resources in this region.

Significance

As our society strives to move towards a more diverse mix of energy resources, interest in harnessing the earth's natural heat generation has increased. While geothermal energy can be a sustainable source of energy, production costs have inhibited private sector interest and most energy generating projects are funded by federal and state agency capital. This is at least partially due to the combination of the high costs of drilling deep wells, poor quantitatively based risk assessment in geothermal systems, and the restricted locations of high geothermal energy potential relative to consumer demand and distribution systems.

The Snake River Plain, Idaho is a known source of high geothermal gradient (Blackwell and Richards, 2004; Blackwell et al., 2011). However, basaltic systems have traditionally been considered poor targets for geothermal exploration, because of the low viscosity of basalt, which facilitates rapid channeling from depth, and consequently, rapid cooling (Nielson et al., 2015). In addition, the Snake River Plain is covered by a shallow cold aquifer that masks the high heat flow (Breckenridge et al., 2012). Yet blind or buried geothermal systems exist, as documented in the case of the MH-2 discovery well (Shervais et al., 2013, 2014). Well-known basaltic geothermal systems include the Puna District in Hawaii (Kinslow et al., 2012) and the rifted basalts in the area of Hengill, Iceland (Harðarson, 2014), which produce 38 MW and 303 MW of electricity, respectively.

The geothermal gradient across the Snake River Plain is not spatially uniform (Blackwell and Richards, 2004; Blackwell et al., 2011). This variability is likely driven by the presence or lack of key elements of a geothermal system: heat and fluid source and recharge, permeability, reservoir, groundwater, and a seal. The existence of those elements depends on the emplacement and depositional history, faults, fractures, and local stresses, and lithologies. Traditionally, prospectivity for geothermal resources has been based on surface manifestations such as hot springs or acid altered ground. The MHAFB site is considered a blind system since there are no such surface manifestations (Breckenridge et al., 2012). The potential for greatly expanding resource targeting, then, lies within subsurface identification of the geothermal system.

To evaluate an energy resource across a range of scales, the petroleum and gas industry has established and championed an industry-wide standard for subsurface analysis termed play fairway analyses. The U.S. Department of Energy Office of Renewable Energy sought proposals to implement oil and gas subsurface evaluation techniques to address uncertainty quantification and reduction in geothermal resource exploration and evaluation, funding opportunity DE-FOA-0000841. Utah State University was one of 11 teams whose proposals were selected. The USU project examines the Snake River Plain as the site for this test (Nielson et al., 2015; Shervais et al., 2015). This exploration project occurs simultaneously to my thesis work, centered on the MH-2 core (Nielson et al., 2015; Shervais et al., 2015; DeAngelo et al., 2016; Garg et al., 2016; Shervais et al., 2016). All of the elements of a relatively shallow and potentially energy generating geothermal resource are present at the MH-2 well location. By integrating the subsurface evaluation with core-based studies, we will be able to calibrate the subsurface characteristics identified as critically important in the risk assessment, in the area surrounding MH-2. The Snake River Plain project was recently chosen in the DOE down select, and is one of six projects going forward to further study the prospects identified in Phase 1. Mountain Home Air Force base is one of the areas to be further examined in this next phase.

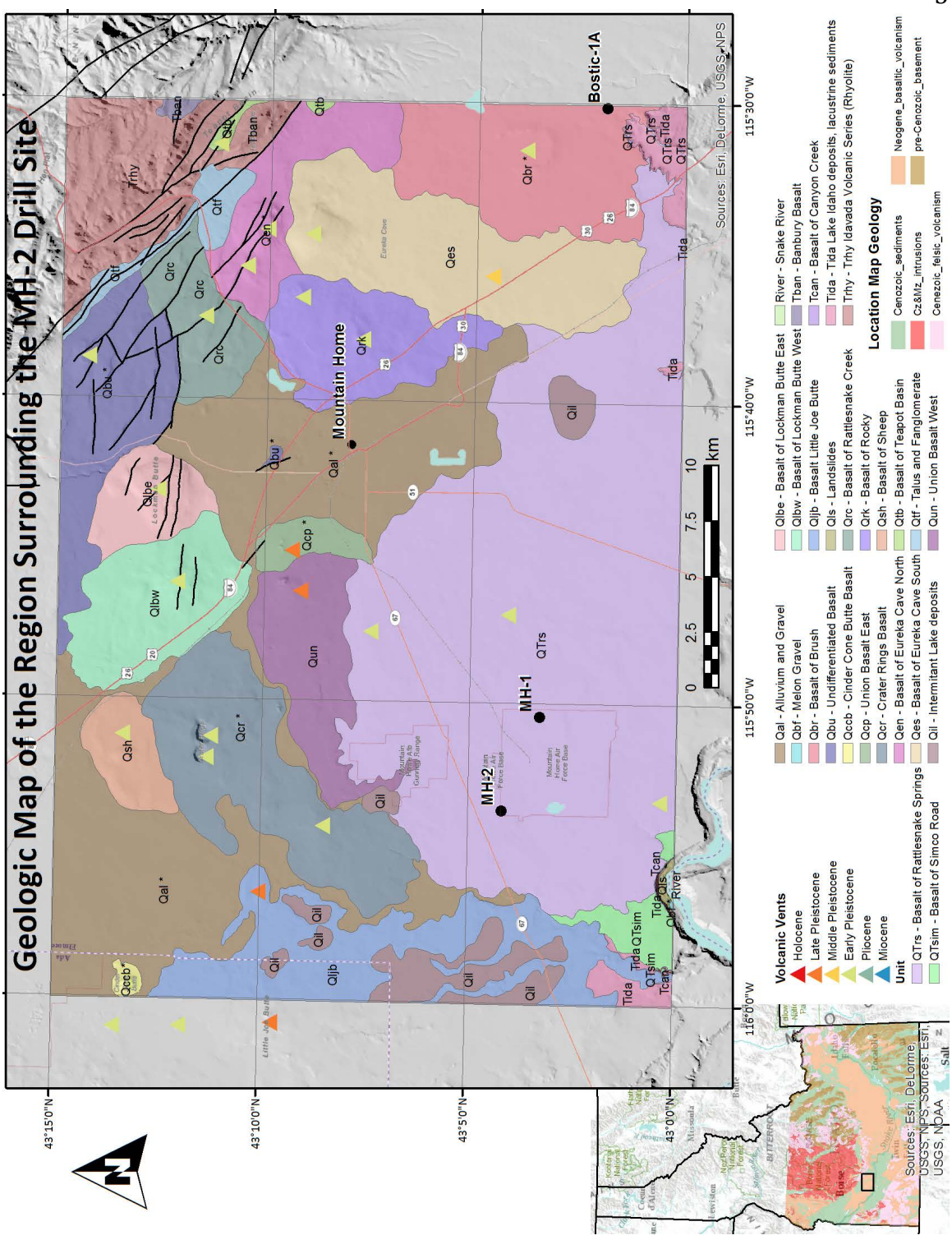

Figure 1. A location map for the MH-2 drill site showing the local surface geology, examined outcrop locations, and other deep drill-holes in the area.

BACKGROUND

Setting

Geology

The Snake River Plain (Figure 1) is divided into the eastern and western segments based on their different geologic histories and structural orientations (Leeman, 1989). The eastern Snake River Plain (ESRP) records the track of the Yellowstone hotspot as the North American plate migrated towards the southwest (Pierce and Morgan, 1992). It contains as many as 6 rhyolitic eruptive centers beginning with the Bruneau-Jarbidge volcanic field (~12 Ma), and continuing with the most recent felsic volcanic activity in the Yellowstone Plateau volcanic field (0.6 Ma) (Pierce and Morgan, 1992; Link and Phoenix, 1996). Basalts then erupted, with basaltic volcanism occurring as recently as late Pleistocene and Holocene in the Great Rift area (Kuntz et al., 1983).

The western Snake River Plain (WSRP) may be a northwest-trending failed intracontinental rift basin, bounded to the north and south by en echelon normal faults striking NW-SE, north of the track of the hotspot (Shervais et al., 2002; Wood and Clemens, 2002). Its proximity and similar orientation to other structures in the Pacific Northwest, such as the Olympic-Wallowa Lineament, suggests that failure occurred along a preexisting weakness in the continental crust as the Yellowstone Hotspot passed (Wood and Clemens, 2002). As the basin subsided it was filled by basaltic volcanic rocks, ash deposits and tuffs, and up to 1.7 km of lacustrine and fluvial sediments (Malde and Powers, 1962; Kimmel, 1982; Shervais et al., 2002; Wood and Clemens, 2002; Beranek et al., 2006). Plume-derived Hawaiian-style

olivine tholeiitic basaltic volcanism occurred in the Miocene and Pliocene (Shervais et al., 2002; Wood and Clemens, 2002). A Plio-Pleistocene system of interconnected lakes filled in the basin with calcareous muds and siliciclastic sediments during a period of diminished volcanism from ~5 Ma to ~2Ma (White et al., 2002; Bonnichsen and Godchaux, 2002). The Pleistocene then saw a resurgence of tholeiitic basalt volcanic activity followed by high potassium basaltic volcanism related to delamination of the lithosphere (Shervais and Vetter, 2009).

The geology recorded in the recovered MH-2 core is believed to be the result of Paleo-Lake Idaho, 3 episodes of basaltic volcanism (late Miocene to early Pliocene, late Pliocene to Pleistocene, and high-potassium late Pleistocene), and ancestral Snake River fluvial sediments (Figures 2 and 3)(Beranek et al., 2006; Kimmel, 1982; Malde and Powers, 1962; Shervais et al., 2002, 2005; Wood and Clemens, 2002). Paleo-Lake Idaho comprises of two successive large lakes represented by (1) Miocene Chalk Hills and (2) the late Pliocene/Pleistocene Glenns Ferry and Bruneau Formations. The thick section of lacustrine sediments near the top of the recovered core is believed to contain the Pliocene-Pleistocene transition, and has been sent to the Limnological Research Center at the University of Minnesota for further analysis.

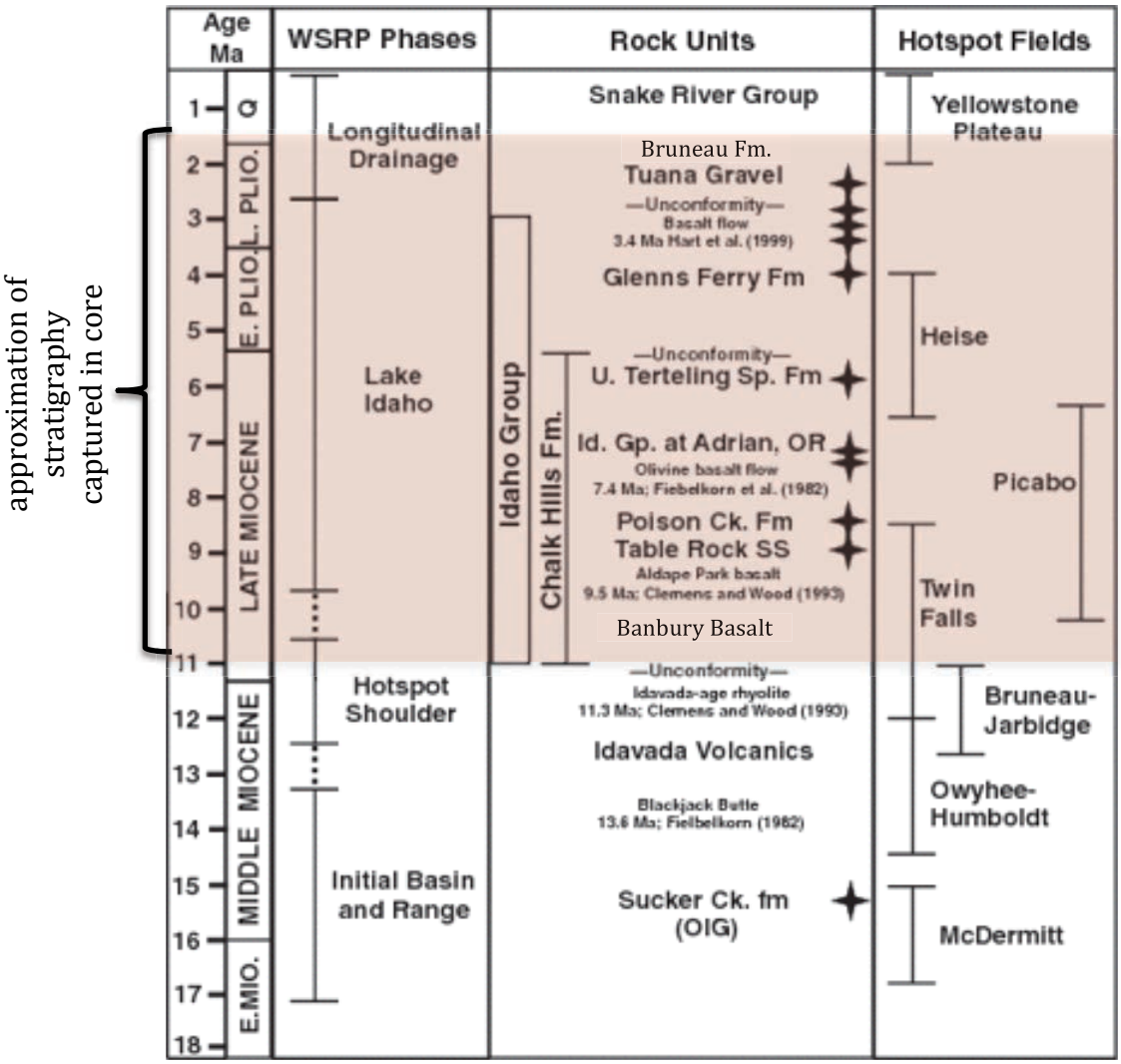

Figure 2. Stratigraphy of the Western Snake River Plain, modified from Beranek (2006). An approximation of the stratigraphy encountered in the MH-2 hole is highlighted.

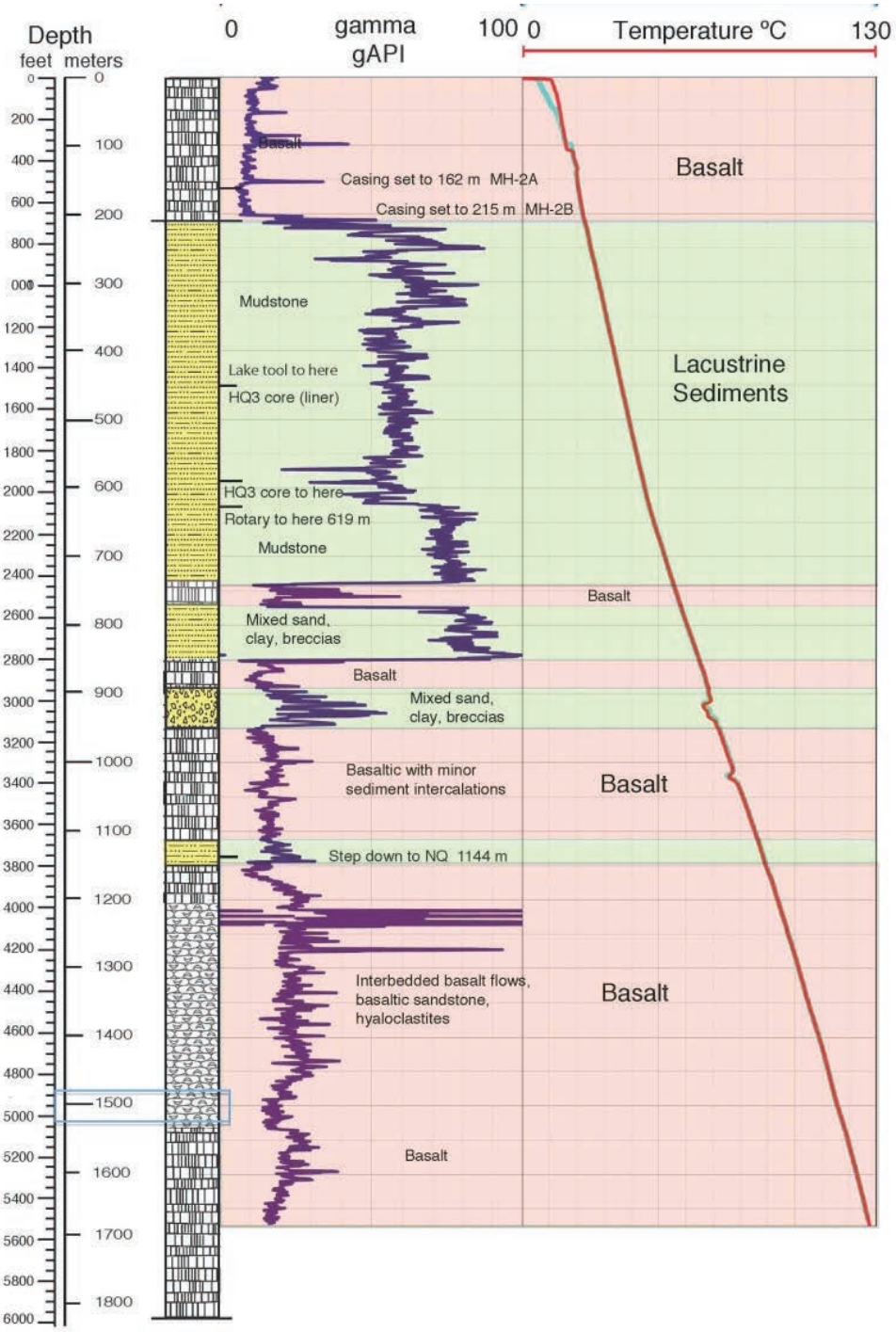

Figure 3. The preliminary lithology log with gamma ray and temperature profile adapted from Shervais (2013). This lithology log was a generalized first order analysis of main breaks in rock type.

Structural Setting

In addition to the steep basin-bounding normal faults to the north and south of the WSRP, the presence of intrabasinal normal faults with similar orientations have been proposed, based on stratigraphic relationships between the MH-1 and Bostic 1a boreholes based on lithologic drillhole logs gravity anomalies, and seismic reflection data (Wood, 1994; Shervais et al., 2002). However, as a result of the younger basaltic volcanic cover in the area and relatively slow slip-rates on the faults, these faults are rarely expressed at the surface. Borehole stress data, acquired from the MH-2 borehole, shows the maximum horizontal stress oriented NE-SW and with a magnitude less than lithostatic stress, consistent with those measured in the northern Basin and Range Province in Nevada (Kessler, 2014), albeit with an $\sim 25°$ clockwise rotation of S_H relative to the closest site in northern Nevada, and at a high angle to S_H orientations in central Idaho. This orientation and relative magnitude of the stress state, as measured in the MH-2 borehole, would produce normal faults striking NE-SW, or perpendicular to the faulting observed in the area. Kessler (2014) proposes that this type of faulting "could be produced as an accommodating antithetical fault in a stepover ramp between two larger en echelon normal faults that strike NW-SE". These stepover fault zones could produce a system of associated open mode fractures, allowing for higher volumes of fluid flow. Identifying the potential for open mode fractures will be an integral part of the USU Geothermal Play Fairway Evaluation.

The MH-2 drill site was chosen (Shervais et al., 2013) based on the presence of an elongated gravity high with its long axis that is sub-parallel to the axis of the

plain based on an interpretation of the Bouguer gravity anomaly map from Idaho gravity data (Kucks, 1999), and from the results of earlier exploratory drill holes. Our exploration and scientific hypothesis was to determine if fractures associated with faults bordering the gravity anomaly are zones of high fluid conductivity and convective heat flow. The gravity anomaly could be a result of underplating of the crust from the intrusion of dense mantle material (Glen and Ponce, 2002; Shervais and Vetter, 2009). Speculation as to the presence of the structures in the graben is that a number of high-angle normal faults exist to produce the accommodation space for a larger volume of early to middle Pliocene basalts in the central part of the western SRP (Arney and Goff, 1982; Arney et al., 1984; McIntyre, 1979; Shervais et al., 2002). The evidence of structures in the subsurface raises the prospect for geothermal development.

Geothermal Setting

Project HOTSPOT investigated 3 distinct geothermal regimes present in the Snake River Plain: 1) the volcanic axis, which is a source of high geothermal gradients, but only below the Snake River Aquifer, 2) low-temperature systems with a broad areal footprint, and 3) a buried or blind high temperature system at the Mountain Home Air Force Base (MHAFB) site. Geothermal exploration and exploitation in the western US has largely been based upon the presence of hot spring activity (Nielson et al., 2015). The MHAFB site is considered a blind system since there are no surface manifestations (such as hot springs or acid altered ground) of the resource that exists.

The MHAFB overlies the margin of the mid-crustal gravity anomaly discussed above, and defined more clearly by Jonathan Glen (USGS, unpublished , pers. comm., 2015), and hypothesized to be a sill complex structure (Nielson and Shervais, 2014). The proposed mechanism of geothermal heat production in the SRP is a mafic sill complex at mid-crustal levels (Shervais et al., 2006). This conceptual model suggests episodic sill emplacement, where multiple sills are injected adjacent to previous ones before initial sills have cooled completely, perpetuating a geothermal heat source.

The Play Fairway analyses (Nielson et al., 2015; Shervais et al., 2015, 2016) extends the results of Project Hotspot to examine the region for geothermal exploration targets. This project assembled pre-existing geologic and geophysical data into a common data platform in ArcGIS, which was then used to determine the location of prospective play types. These analyses screened areas for thermal source, reservoir, seal, and present a risk-based assessment of the plays. Owing to the favorable risk the Mountain Home Snake River Plain mid-crustal basalt complex play is one of the areas thought to be prospective.

Previous Work

The MH-2 well was drilled as part of a Utah State University led drilling project, Project Hotspot (Shervais et al., 2011, 2013, 2014). The main goal of Project Hotspot was to document the volcanic and stratigraphic history of the Snake River Plain and to investigate geothermal potential in three distinct regimes of the Snake River Plain. The Kimama and Kimberly drill sites were strategically chosen to

sample a nearly continuous chronologic record of emplacement as a result of the northeast migration of the Yellowstone Hotspot relative to the North American Plate. The Mountain Home drill site was chosen to sample the thick package of lacustrine sediments that are believed to have captured the Pliocene-Pleistocene transition. Geomechanical analyses and a first-order analysis of rock types was the focus of Kessler (2014), no detailed lithologic analysis of the MH-2 core has been performed. A finer scale analysis of the lithologies and the geologic interpretation of those lithologies is the main goal of this thesis project.

Interest in geothermal potential in the WSRP was sparked by a bottom hole temperature of 175°C recorded in an oil and gas wildcat well, Bostic-1A (Armstrong et al., 2013). The Bostic-1A hole, drilled in 1973, is 31.7 km east of MH-2 (Figure 1), also in the WSRP geologic province, and drilled to a total depth of 2950 m bgs (Arney et al., 1984). The Mountain Home Air Force Base became interested in exploiting the high geothermal gradient of 59°C/km encountered in the Bostic-1A hole, and drilled a geothermal exploratory well of their own, MH-1. The MH-1 hole is 4.6 km southeast of MH-2 (Figure 1). Drilled in 1986 to a total depth of 1342 m, the Air Force hoped to supply a heat source to military housing on the base (Lewis and Stone, 1988). A temperature of 93°C was recorded at a depth of 1219 m bgs (69°C/km geothermal gradient) but lacked artisanal flowing water. With technology that was available at the time, it could not be used for its intended purpose, and as a result the hole was plugged and abandoned (Armstrong et al., 2013). Increased efficiencies in geothermal energy development (e.g., binary power systems) suggested that temperatures hot enough to produce energy at a depth of 1524 m bgs

at the MHAFB, became the motivation for the site selection of the MH-2 hole (Armstrong et al., 2013). The proximity of these two wells to the MH-2 drill site presents a great opportunity to extrapolate subsurface lithology continuity and infer structures present but not observed at the surface.

METHODS

The geologic characterization of the MH-2 borehole is based on core observations, compilations of previous core descriptions, drill-site observational logs, and X-ray diffraction (XRD) and thin section analysis. Lithologic contacts were delineated by 1) rock type, aided by the wireline logs and 2) rock texture exhibited in the core. Sampling for XRD and thin sections was based on these lithologies and also mechanical stratigraphy identified (Kessler, 2014). We delineate 5 litho-stratigraphic units based on dominant lithologies, identified in the MH-2 core, that reflect significant tectonic and depositional environment changes as the landscape evolved. These stratigraphic units are interpreted to fit into geologic models of the WSRP proposed by Shervais (2002) and Wood and Clemens (2002).

Core Descriptions

The MH-2 borehole was cored with diamond drill coring methods. Core recovery (length recovered/length cored) was 94.8% (Delahunty et al., 2012). Drilling was performed by DES, Inc., with a truck-mounted Atlas Copco CS-4002 drill rig. Upon recovery, the core was cut into 0.61 m sections and boxed for storage. The core boxes contain 3 PQ (85 mm diameter to 455 m) sections and 5 sections each of HQ (63.5 mm diameter to 1144 m) and NQ (48 mm diameter to TD 1821 m) (Plate 1). Two holes were drilled, MH-2A and MH-2B. The first hole, MH-2A, was abandoned after the drill rods became stock at 587.3 m. Core was recovered from 161.5 m to 587.3 m. MH-2B was drilled 7 m east of the abandoned hole and core recovery began at 618.7 m to a completed depth of 1821.5 m (Delahunty et al.,

2012). Core from 214.1 m to 625.6 m was sent to the LacCore facility of the Limnological Research Center at the University of Minnesota for analysis. This section of core was not directly examined as part of this thesis work, and relied on previous descriptions of the core (Shervais, 2014). As a result this section is slightly less emphasized. The remainder of the core is currently stored on the campus of Utah State University, in Logan Utah, but will ultimately be transferred to the U.S. Geological Core Repository in Denver, CO.

I examined and logged the entire core, over the depth intervals 161.5 – 214.1 m bgs and 625.6 – 1821.5 m bgs, stored on-campus at USU. I delineated the litho-stratigraphy based upon the lithologies present and differing textures within lithologies. In conjunction to core examinations, I correlated lithology descriptions with the down-hole wireline logs. Gamma-ray logging was performed from the surface to 1675 m bgs, and a suite of open hole logs below the HQ rods from 1165 to 1675 m bgs were acquired by the Operational Support Group of International Continental Drilling Program (Plate 1). At the time of logging 1675 m bgs was TD. For this work I examined the master gamma ray log, spectral gamma, sonic velocity logs, and resistivity logs and correlated to the characterized lithologies.

Thin Section Analysis

Thin sections were prepared from 27 core samples (Table 2). I examined the thin sections with a petrographic scope for mineral and rock type identification. Sample selection for thin section preparation was biased towards alterations and

secondary rock types, as they can be used for identifying hydrothermal temperatures during the time of mineralization (not a part of this work).

X-ray Diffraction

Powders were prepared from the same samples from which the thin sections were prepared (Table 2). X-ray diffraction analysis was performed on 29 samples with an X'Pert Pro Diffractometer system running at 45KV/40Ma with copper tubing. Measurements were obtained with a continuous scan from 2° - 75° with 0.02° interval for a period of 1 second per interval. X'Pert Data Collector and X'Pert High Score software were used in data analyses to determine mineral compositions present.

Outcrop Analogues

I describe outcrop analogs in proximity to the MH-2 hole, along the bluffs of the Snake River (Figure 1). Based on the elevation of the top of the borehole, the elevation of the outcrops, and the stratigraphic position of the outcrops (overlying Chalk Hills), I have determined that the outcrops are not directly represented in the MH-2 core. Outcrop representations of flows below the Chalk Hills were not observable in this area. However, much insight was gained into volcanic facies, stratigraphic and textural relationships, and basaltic flow interactions with a water body. An annotated representation of what I observed is shown in Figure 4.

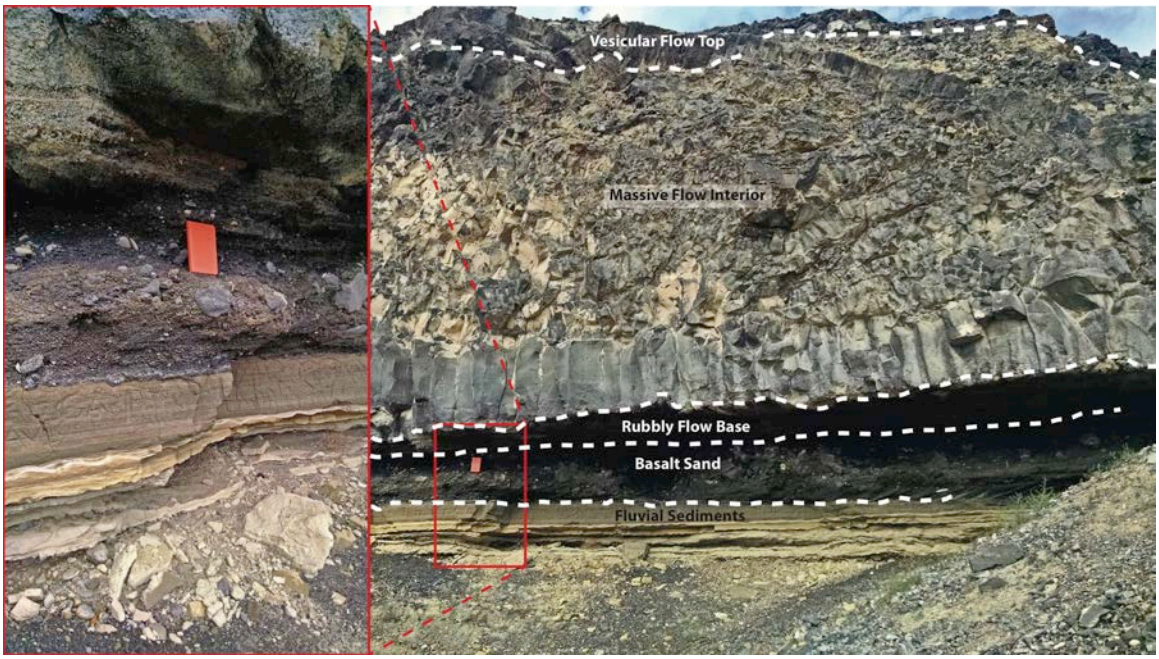

Figure 4. An outcrop exposure of analogous strata to the MH-2 core, 1 mile north of C.J. Strike Dam (42°57'40.72"N, 115°58'23.02"W). This outcrop is composed of a single flow with three distinct flow facies or flow units. At the base of the flow is a poorly-sorted basalt sandstone. This flow overlies a series of fluvial and lacustrine sediments. Soft sediment deformation has occurred in the lacustrine sediments, indicating dewatering, possibly as a result of the added overburden of the basaltic flow.

RESULTS

Core logging results indicate that the MH2 core is dominated by basalts in the lower part of the core (853 – 1821 m bgs), and the lacustrine sedimentation in the upper reaches of the core (213 – 853 m bgs) that filled the basin (Appendix A; Plate 1). At least 67 individual basalt flows were identified (Plate 1; Appendix A). In many parts of the core, we observe evidence for an over print of brecciation and alteration. Intercalated basalt sandstones are present throughout the core, and not evenly distributed. The nearly 700 m of lacustrine sediments near the top of the core are segmented by a change in dominant grain size and mineralogy.

I delineate five litho-stratigraphic units based on the dominant lithology, from bottom to top: 1) sub-aerially erupted basalts, 2) sub-aqueously erupted basalts, 3) deep water environment muds, 4) siliciclastics, and 5) subaerially emplaced basalts.

Wireline logging results show that variations in the gamma-ray logs are useful for identifying lithologic breaks between volcanic and sedimentary rocks. Sonic velocity logs can be used to differentiate between unaltered basalts and zones of altered and brecciated basalts. The resistivity log is also useful for identifying where breccias and altered zones in the basalt exist, but potentially at a higher resolution, which may be useful for delineating more subtle features such as flow contacts and periods of non-emplacement.

Lithology

There are five primary lithologies and two lithologies as a result of secondary processes within the MH-2 core (Table 1 Figures 6 – 8). The primary lithologies in the MH-2 drillhole are: 1) basalt, 2) hyaloclastite, 3) basalt sandstone, 4) silt/sand mixtures, and 5) diatomaceous mudstone. Secondary lithologies are: 1) altered basalt and 2) brecciated basalt (Figures 3, 6, 7, 8; Table 1; Appendix A).

Primary Lithology

Basalt

The 67 individual basalt flows are delineated by attributes such as density of vesicles, percentage of glass, oxidation state, vesicle structures, jointing, crystal texture and presence of rubble. Ideally an individual flow will be represented in core by 3 distinct sections: 1) an upper crust, 2) a core, and 3) a lower crust (Figure 5) (Self et al., 1998). In this model, the upper crust of a flow is vesicular and glassy and the upper most portion of the upper crust will exhibit relatively higher oxidation. The core of a flow is massive and has much lower abundance (<10%) of glass then the crusts with very few vesicles. Vesicles that do exist in the core of a flow are discrete cylinders or sheets, as a result of silica residuum (Self et al., 1998). The base of a flow is known as the lower crust. It is nearly as vesicular as the upper crust, very glassy, and often rubbly. All, some, or only 1 section of an idealized individual flow may be observed within the MH-2 core, making delineating a flow more nuanced than the idealized case. I could identify at least 67 individual flows, based on the Self et al (1998) flow-section criteria when possible, and by variability in texture and/or

Table 1. – Summary of lithologies encountered in the MH-2 borehole

Lithology	Description
Basalt	This includes vesiculated, aphanitic, and fine-grained crystalline textures. It is composed of plagioclase, olivine, pyroxene, Fe and Ti oxide minerals, and glass. Dry color varies; moderate light gray, grayish olive green, grayish black and nearly black. Plagioclase and olivine phenocrysts are common.
Altered basalt	Same as fresh basalt but bulk rock is composed of >30% alteration minerals, most commonly zeolites, calcite, clay, and analcime. Phenocrysts of olivine are partially or completely replaced with clay. Clays are mostly smectite and in one sample kaolinite was detected. Zeolite, calcite, and pyrite, exist as void and fracture fill. Clays exist as degradation interstitial of glasses and replacement of olivine.
Brecciated basalt	Comprises angular gravel sized basalt fragments in matrix of finer basalt clastic ground mass or mineralized by alterations. Evidence of alterations filling and mineralizing open voids rapidly.
Hyaloclastite	A low density tuffaceous altered basalt. It is rich in glass and comprised of angular and faceted clasts millimeter to centimeter in size. Differing distinction from basalt sand is the high abundance of glass, and lack of sedimentary structures. Clasts are also more angular than those in basalt sands.
Basalt sandstone	Sand deposits with clasts derived from basalt rock. Clasts range from angular to rounded, and from very fine sand to coarse gravel. Some deposits display sedimentary structures such as bedding planes and sorting.
Silt/sand mixtures	Ranging from predominantly silts and fine sands to less common coarse sands and gravels. Clasts are composed of quartz, feldspars and micas, with calcareous matrix.
Mudstone	Clay and silt, highly calcareous, ranges in dry color; light olive brown, dusky yellow, light olive gray, and dark yellowish brown. Laminations are common, possibly varves. Core breaks along bedding plains. Some sections are shaley and fissile.

Table 2. X-ray diffraction analysis results.

Depth (m bgs)	lithology	Plagioclase	Olivine	Pyroxene	Oxide	SiO2	Calcite	Zeolite	Analcime	Chalcopyrite	Aerinite	Clay	Other
168.22	basalt	x (An)	x				x (siderite)						
212.48	basalt sand	x (labradorite)				x (low quartz)							
758.13	basalt	x (labradorite)					x	x (Na)	x	x			
848.75	mudstone						x	x (Na)					
849.72	mudstone						x	x (clinoptilolite)		x			
890.69	altered basalt	x (labradorite)					x	x (Na)					
946.95	hyaloclastite basalt						x	x (Na)	x				
1077.68	basalt sand							x (Na)	x			x smectite	
1195.41	basalt sand						x (ankerite)	x					
1242.94	basalt	x (An)		x (Augite)				x					
1255.77a	basalt				x (Mg Al2 O4)				x		x	x smectite	
1255.77b	basalt						x	x (Na)				x smectite	
1277.60	basalt	x (labradorite)		x (diopside)				x				x smectite	
1323.17	basalt			x (clino)				x					hisingerite
1323.62	basalt	x (Ab)		x (diopside)		x (cristobalite)						x smectite	
1325.73	basalt	x (An)			x (Fe+2 Fe2+3 O4)						x		
1372.33	brecciated basalt			x (Fs)				x (Na)	x				
1405.95	altered basalt	x (An)		x (diopside)	x (Fe+2 Ti O3)							x smectite	
1466.48	basalt	x (An)	x					x (K)					
1510.80	brecciated basalt								x			x smectite	
1554.54	basalt	x (labradorite)			x (Fe+2 Ti O3)							x smectite	phosphate
1658.08	basalt	x (An)	x		x (Zn Fe2 O4)								
1676.45	basalt	x (An)		x (En)								x smectite	
1731.32a	altered basalt	x (labradorite, An)										x smectite	
1731.32b	altered basalt							x		x		x smectite	
1736.11a	basalt sand	x (An)					x (ankerite)	x (Ca)					
1736.11b	basalt sand						x	x (Ca)			x		
1744.98	brecciated basalt	x (Ab)						x					
1751.13a	basalt	x (Ab)						x (Na)					
1751.13b	basalt	x (Ab)						x (K)				x kaolinite	
Blue = Primary													
Red = Secondary													
thermal zone													

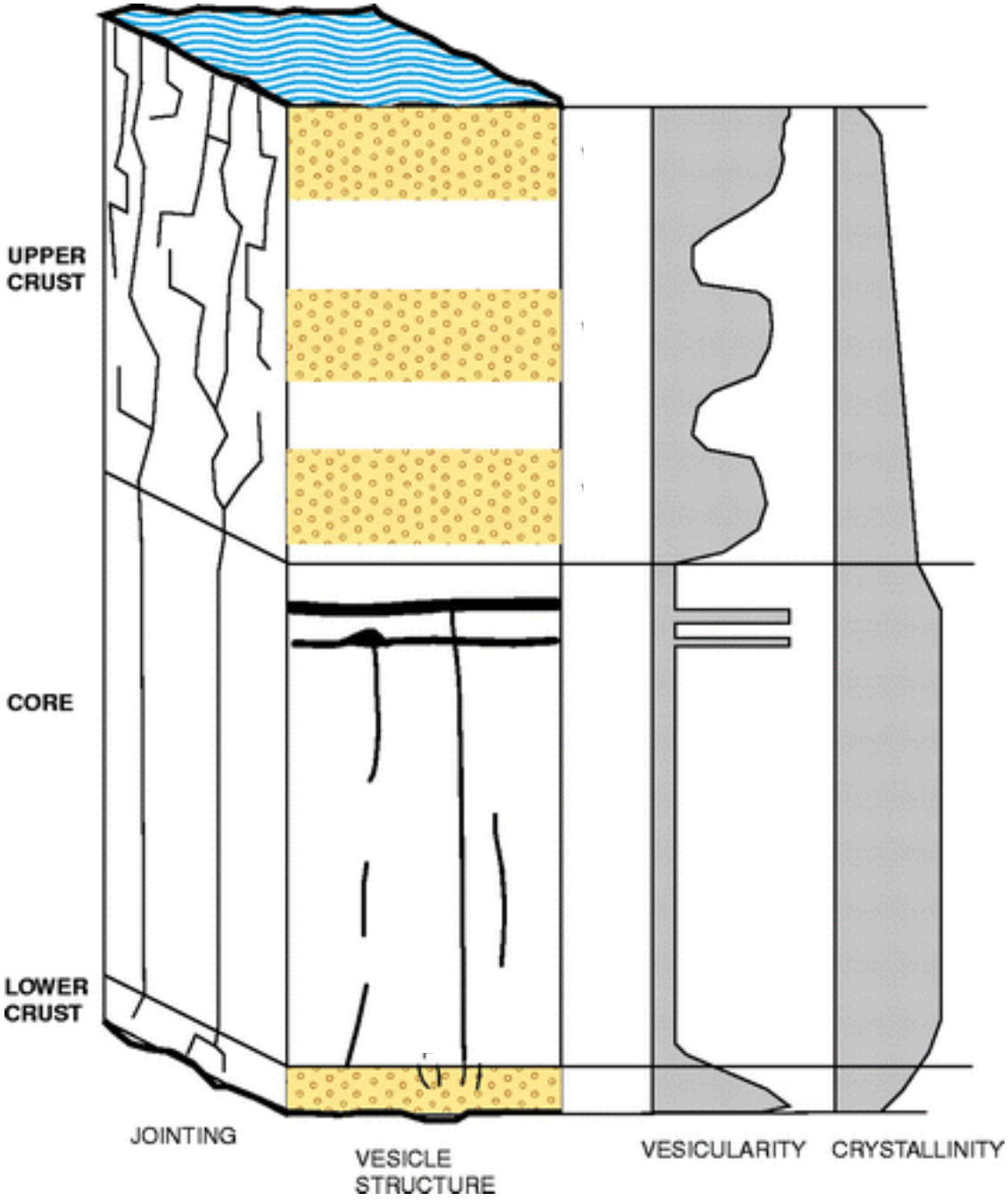

Figure 5. A diagram of an idealized lava flow, with a vesicular upper crust, a core with localized vesicles, and a vesiculated and rubbly lower crust. Adapted from Self et al (1998).

color when flow-sections were not easily identifiable. Flows vary in thickness from 1.5 m to 103 m.

In core samples, the dry color of basalt ranges from moderate light gray, to grayish olive green, to grayish black, and nearly black. Plagioclase phenocrysts are commonly observed and in some cases display a variolitic texture, surrounded in aphanitic groundmass in crystalline zones (Figure 6). In upper and lower vesiculated boundaries of a flow, mineral-filled vesicles and vugs occur. Pyrite, and calcite crystals fill macro-voids such as vugs. In Unit 1, light gray basalts are mottled, interpreted to be a degradation of olivine phenocrysts to clays.

Thin section analysis reveals that the basalts are composed of plagioclase, olivine, oxides, clinopyroxene, and glass. Abundant plagioclase phenocrysts are present, commonly on the order of 2 – 5 mm in length, with the largest being centimeter scale, and commonly in a sunburst radial pattern (Figures 9C, 11A, B, E, 12A, C, D, and 13 C). Olivine and clinopyroxene grains are small and equant, and ilmenite needles are present (Figures 9A, 12A, C, D, and E). These main constituents are surrounded by glass, and acicular plagioclase and clinopyroxene (Figures 11A, B, C, and E). A “browning” color effect is observed in thin section in some basalts (Figures 10E, 12A, C, D, and E). This is a result of olivine degrading, probably into iddingsite, a fine-grained intergrowth of smectite clay (Katherine, 1987). Orange and brown clay is observed in veins or fluid flow pathways best shown in thin sections at 1277.60, 1323.17 and 1323.62 m bgs (Figure 11A, B and C). In vesicular basalt, clay rims the vesicles (Figure 9C). This is commonly observed as a degradation of glassy rinds that rim vesicles as a result of rapid cooling (Minitti et

al., 2007). Sparry calcite is ubiquitous throughout most of the thin sections analyzed. It is present as a secondary mineral filling primary porosity in vesiculated basalt (Figure 9C).

Plagioclase observed in thin section was identified in XRD analysis as labradorite in most samples. A noteworthy exception is the basalts in the geothermal zone at 1745 m bgs (Table 2). Here albite variety plagioclase is predominate (Table 2). The clay observed in thin section is identified as smectite in XRD, also except in the thermal zone, where kaolinite is detected (Table 2). Consistent with the thin section analysis, calcite is a very common secondary mineral, but slightly less common than zeolites, which was identified in over 70% of the samples. Also of significance was the presence of analcime in 6 samples. Analcime, commonly found among zeolites, is a sodium aluminum tectosilicate, which occurs as cavity or vesicle filling (Table 2). This mineral assemblage, which also includes chalcopyrite, indicates strong hydrothermal alteration.

Hyaloclastite

Zones of glassy basaltic breccia and tuff-like low-density rock composed of sintered tephra with faceted angular clasts millimeter to centimeter in size are termed hyaloclastites (Figure 7B). The term hyaloclastite refers to a hydroclastic rock formed by fragmentation of lava by non-explosive thermal granulation in the presence of water (Werner and Schmincke, 1999). These deposits can be layered or chaotic. They are composed of palagonitized glass (usually sideromelane or tachylite) fragments (Werner and Schmincke, 1999). In the MH-2 core hyaloclastites

Figure 6. Unaltered basalt with variolitic phenocrysts of plagioclase and olivine, 164.9 (top right) – 166.6 (bottom left) m bgs.

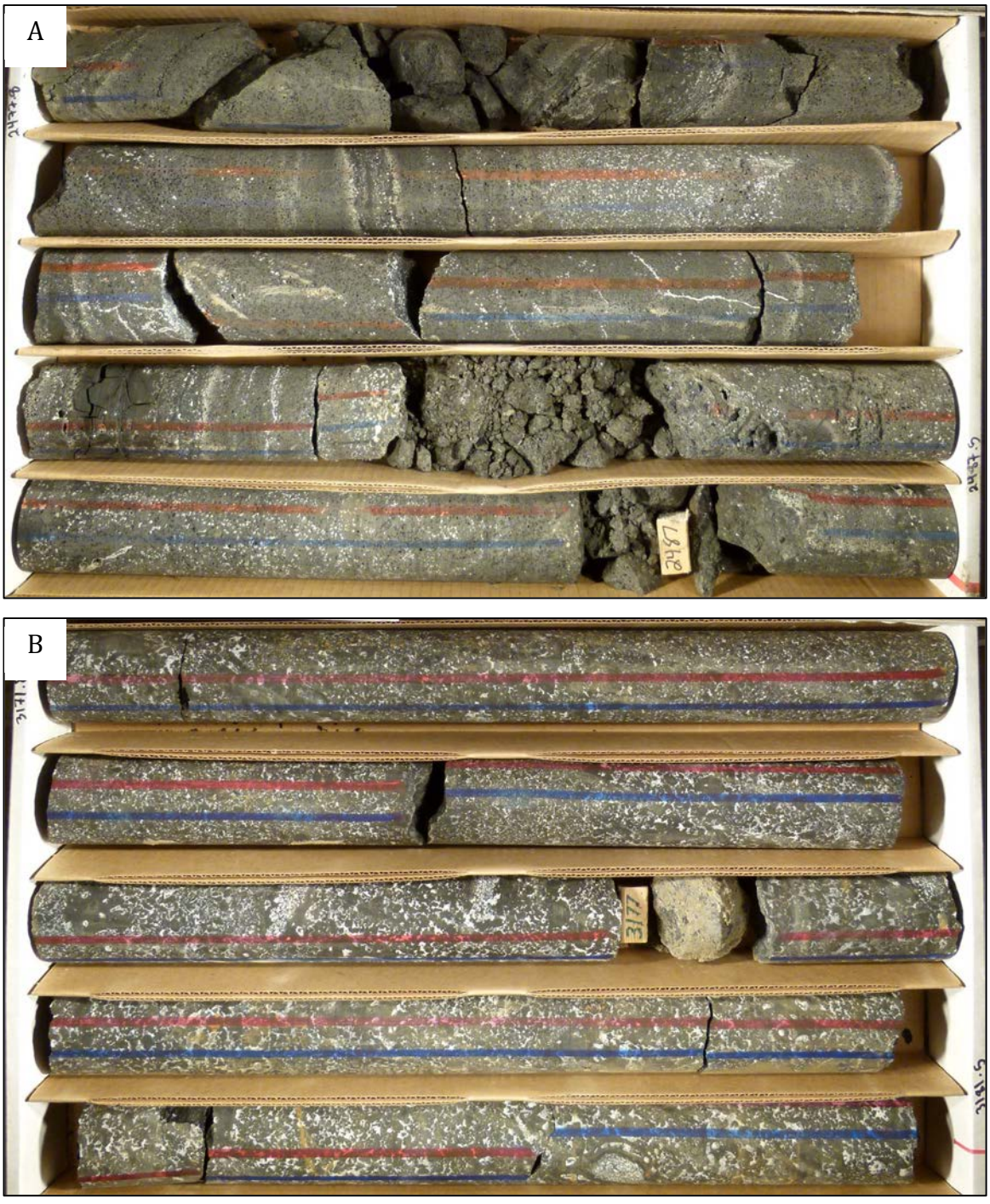

Figure 7. A (top image): Basalt sand in the MH-2 core, 755.2-758.1 m bgs. Bedding planes are observed, grain sizes are coarse indicating a high energy, probably fluvial, environment. B (bottom image): Hyaloclastite in the MH-2 core, 966.7-969.7 m bgs. Faceted angular clasts, millimeters to centimeters in size, make up this glassy tuff. Primary porosity is filled with secondary calcite, zeolites, and analcime.

Figure 8. A basalt flow/lacustrine mud contact in the MH-2 core, 769.0-772.0 m bgs. The basalt overlies the lake mud.

consist of angular shards of glass and blocky shards of basalt rock fragments that range from non-vesicular to vesicular. Vesicles in the blocky shards are elongate with diameters < 1 mm (Figure 7B). Mineral grains are too fine to be observed in core samples. The hyaloclastite deposits occur with other lithologies associated with aqueous environments, such as mudstones and basalt sandstones.

Basaltic Sandstone

Sandstones composed of basalt clasts are present throughout the MH-2 core (Figures 3, 7A, and 9). The primary characteristics that discriminate basalt sands from hyaloclastites are the degree of rounding in the clasts, sorting, and sedimentary structures associated with transport processes (*e.g.* cross

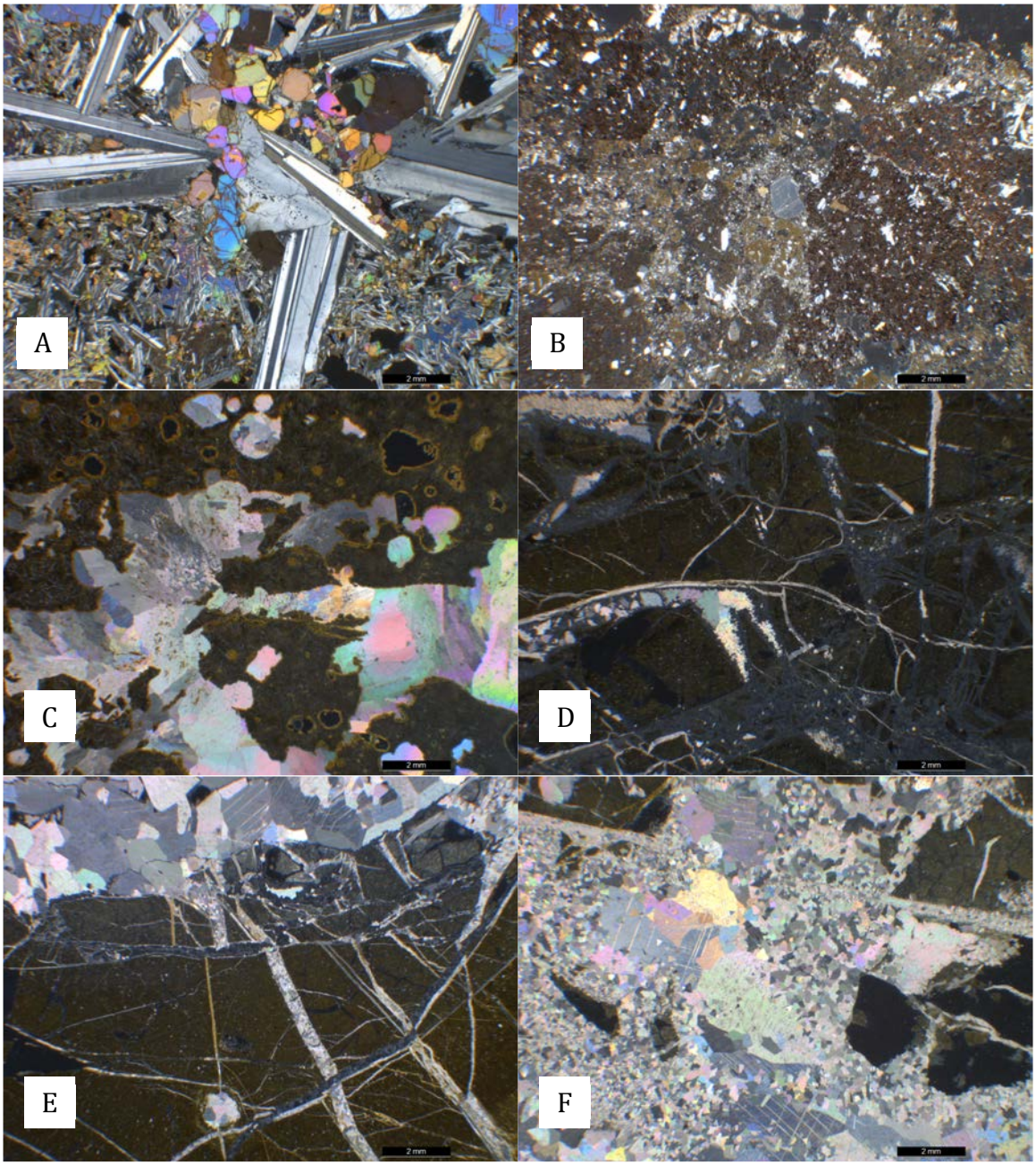

Figure 9. Thin section images under cross-polarized light; field of view is 15 x 11.2 mm in each image. A) 168.28 m bgs, massive basalt with plagioclase laths and ground mass, olivine, pyroxene and glass. B) 212.48 m bgs, basalt sand. C) 758.13 m bgs, vesicular basalt with glassy ground mass, vesicles are rimmed with smectite and filled with calcite. D) 848.75 m bgs, fractured mudstone, fracture fill zeolites, calcite, and chalcopyrite. E) 849.72 m bgs, fractured mudstone, fracture fill zeolites (clinoptilolite), calcite, and chalcopyrite. F) 849.72 m bgs, vein fill in a fractured mudstone, zeolites (clinoptilolite), calcite, and chalcopyrite.

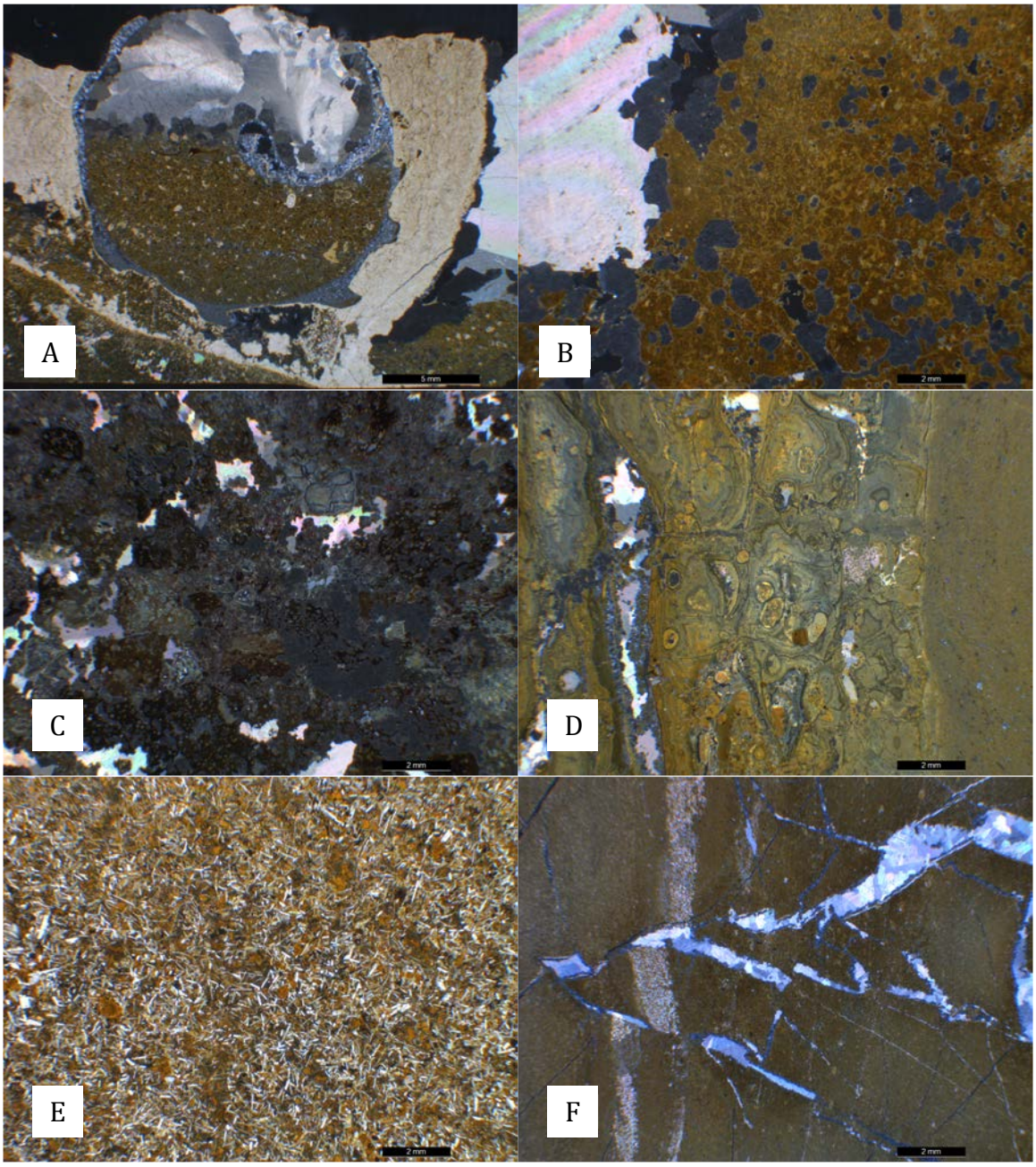

Figure 10. Thin section images under cross-polarized light; field of view is 15 x 11.2 mm in each image. A) 890.69 m bgs, fracture fill in a highly altered basalt. B) 946.95 m bgs, hyaloclastite basalt, glass, clay, and calcite. C) 1077.68 m bgs, basalt sand, calcite, zeolite, analcime, and smectite. D) 1195.41 m bgs, basalt sandstone, zeolite, analcime, calcite. E) 1242.94 m bgs, basalt, plagioclase, augite, pyroxene, oxides and intergranular smectite. F) 1255.68 m bgs, mudstone, with at least 2 episodes of fracturing, calcite in fracture fill.

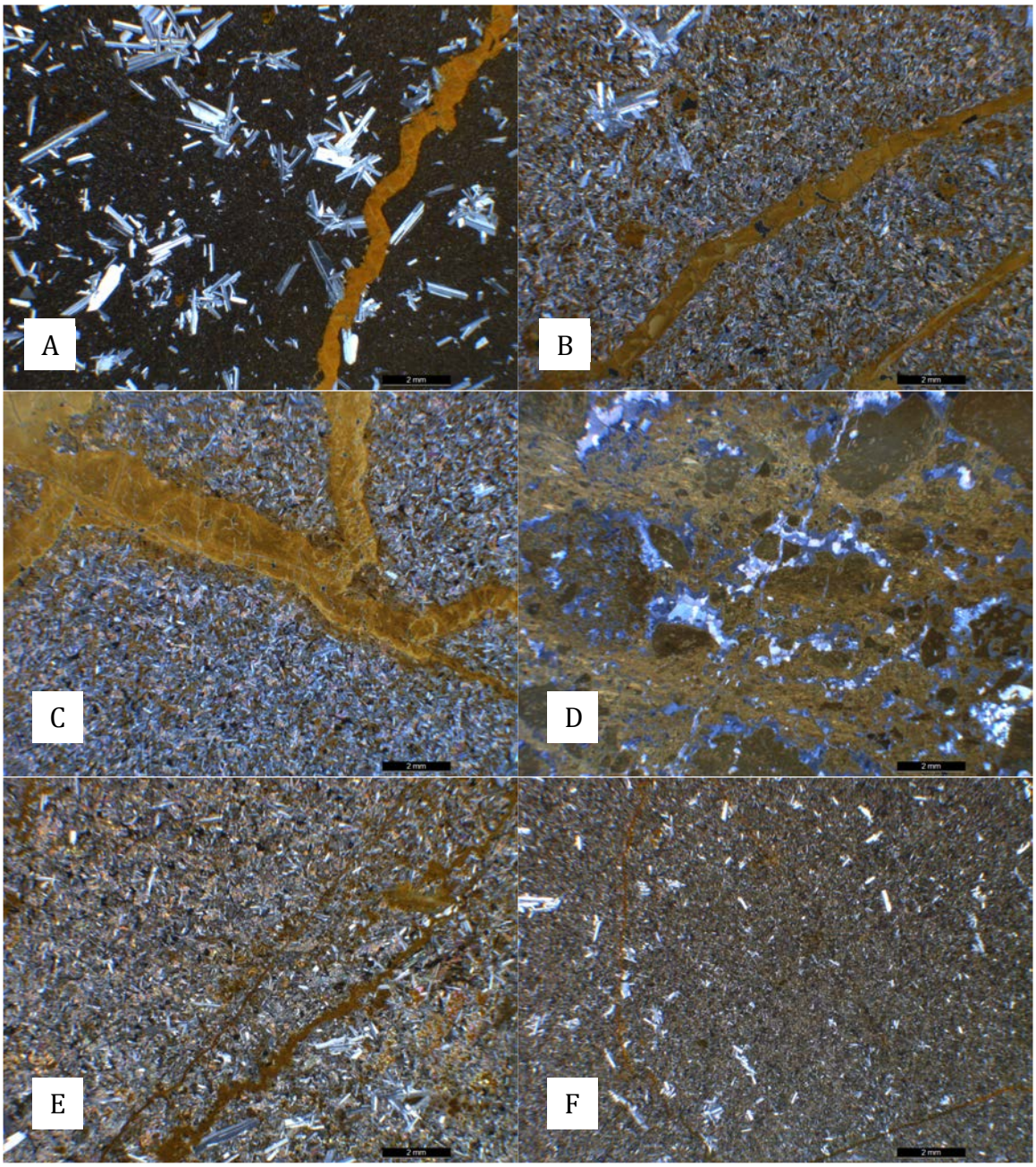

Figure 11. Thin section images under cross-polarized light; field of view is 15 x 11.2 mm in each image. A) 1277.60 m bgs, basalt, plagioclase laths and ground mass, smectite in vein. B) 1323.17 m bgs, basalt, plagioclase, olivine, oxide, and clinopyroxene, smectite in vein. C) 1323.62 m bgs, basalt, plagioclase, olivine, oxide, and pyroxene, smectite in vein. D) 1325.73 basalt, rubbly flow base, plagioclase, oxide, calcite fracture fill. E) 1325.82 m bgs, basalt, plagioclase, olivine, pyroxene, oxide, zeolite, and smectite in vein. F) 1405.95 m bgs, altered basalt, labradorite, pyroxene, oxide, and smectite.

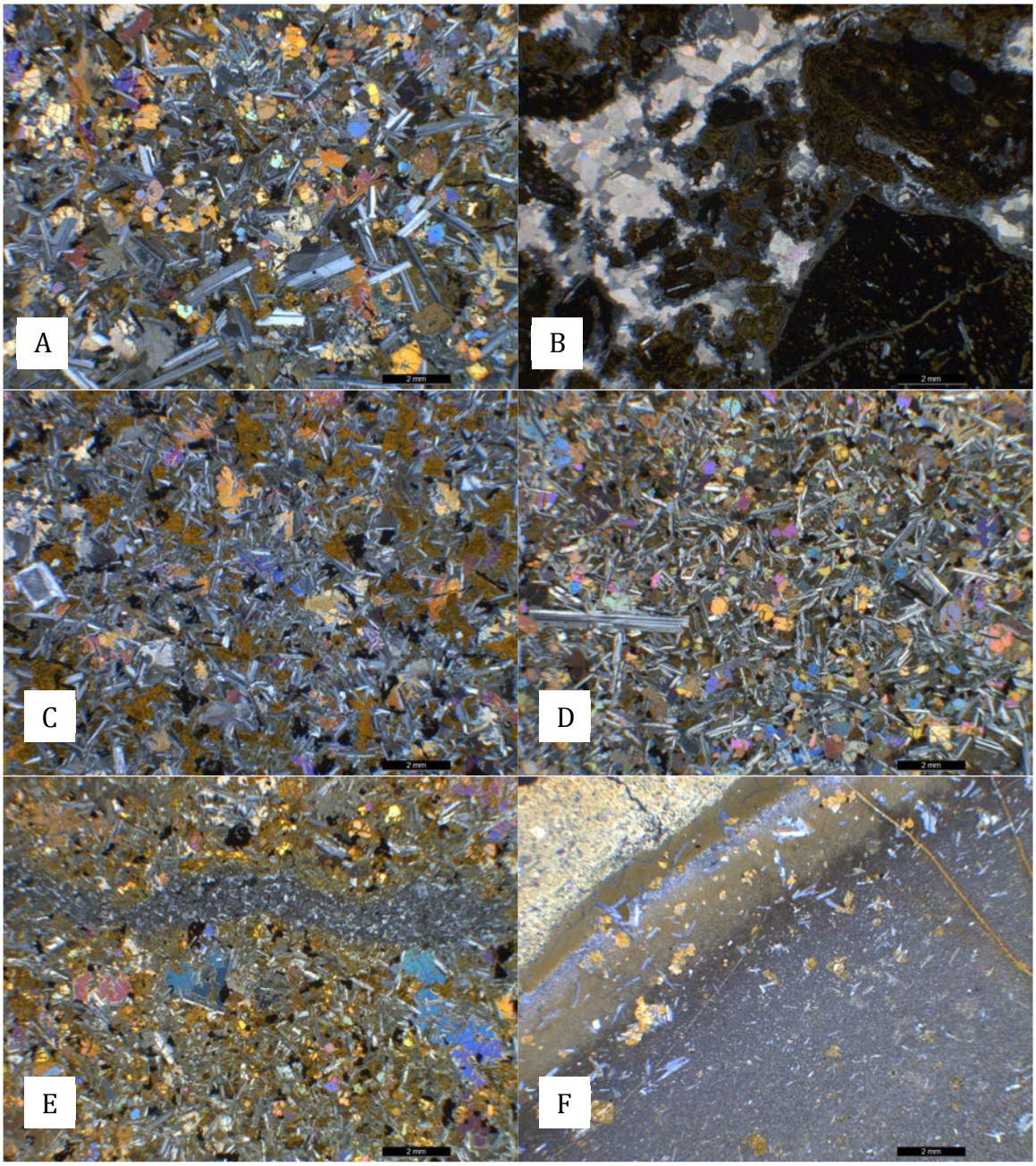

Figure 12. Thin section images under cross-polarized light; field of view is 15 x 11.2 mm in each image. A) 1466.48 m bgs, basalt, plagioclase, olivine, pyroxene, oxide, zeolite, and smectite. B) 1510.82 m bgs, brecciated basalt, basalt clasts in matrix of calcite, analcime, zeolite, and smectite. C) 1554.54 m bgs, basalt, plagioclase, olivine, pyroxene, oxide, smectite, and phosphate. D) 1658.08 m bgs, basalt, plagioclase, olivine, oxide, pyroxene, smectite. E) 1676.45 m bgs, basalt, plagioclase, pyroxene, olivine, oxide, smectite. F) 1731.17 m bgs, highly altered basalt, plagioclase, zeolite, chalcopyrite, and smectite.

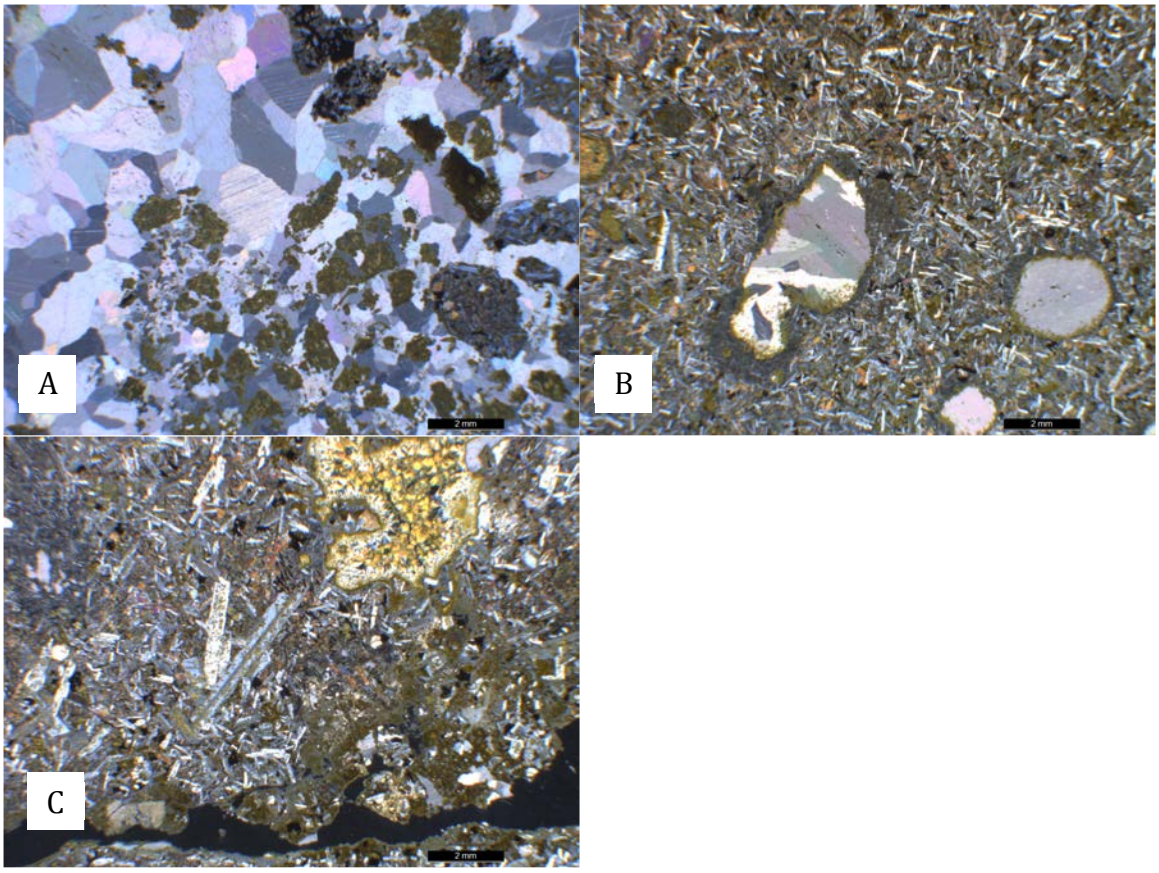

Figure 13. Thin section images under cross-polarized light; field of view is 15 x 11.2 mm in each image. A) 1735.96 m bgs, basalt sand, basalt clasts in calcareous cement. B) 1744.98 m bgs, basalt plagioclase, olivine, pyroxene, oxides. C) 1751.08 m bgs, basalt, plagioclase, olivine, pyroxene, oxides. Thin sections B and C are from the thermal zone, where artesian flowing hydrothermal water was encountered. Of significance, XRD analysis results show the plagioclase in these samples has been altered to albite, and clays present in this zone are kaolinite.

bedding)(Figure 14); otherwise, they are very similar to the hyaloclastites. Clasts in the basalt sandstones range from angular to rounded, and from fine sand to coarse gravel in size. They are cemented by calcite (Figures 10C and 13A). These deposits are much lower density than primary basalts.

Silt and Sandstone Mixtures

These deposits were not directly observed in this work, as the core containing this lithology was not available for examination; they are limited to the top portion of the core (213 – 549 m bgs) (Plate 1). However, they have been previously described as being silicic and felsic in origin, primarily composed of quartz and feldspars with common micas, cemented by calcite (Shervais, 2014). These deposits are primarily fine-grained silts and fine sands and intercalated coarse sands and fine to coarse gravels are also present (436 – 441 m bgs). They are moderately to poorly consolidated, and range from poorly to well sorted.

Diatomaceous Mudstone

Mudstones in the upper section of the core are composed of highly calcareous, poorly consolidated to consolidated clay rich mud (Figure 15). Textures range from laminar with fracturing along bedding planes, to argillaceous deposits with no apparent bedding planes and conchoidal fracturing, and in places the mudstone is fissile and shaley. The commonality in the varied sub-lithologies is that they are very fine-grained (clay and silt) requiring a quiet deep-water depositional

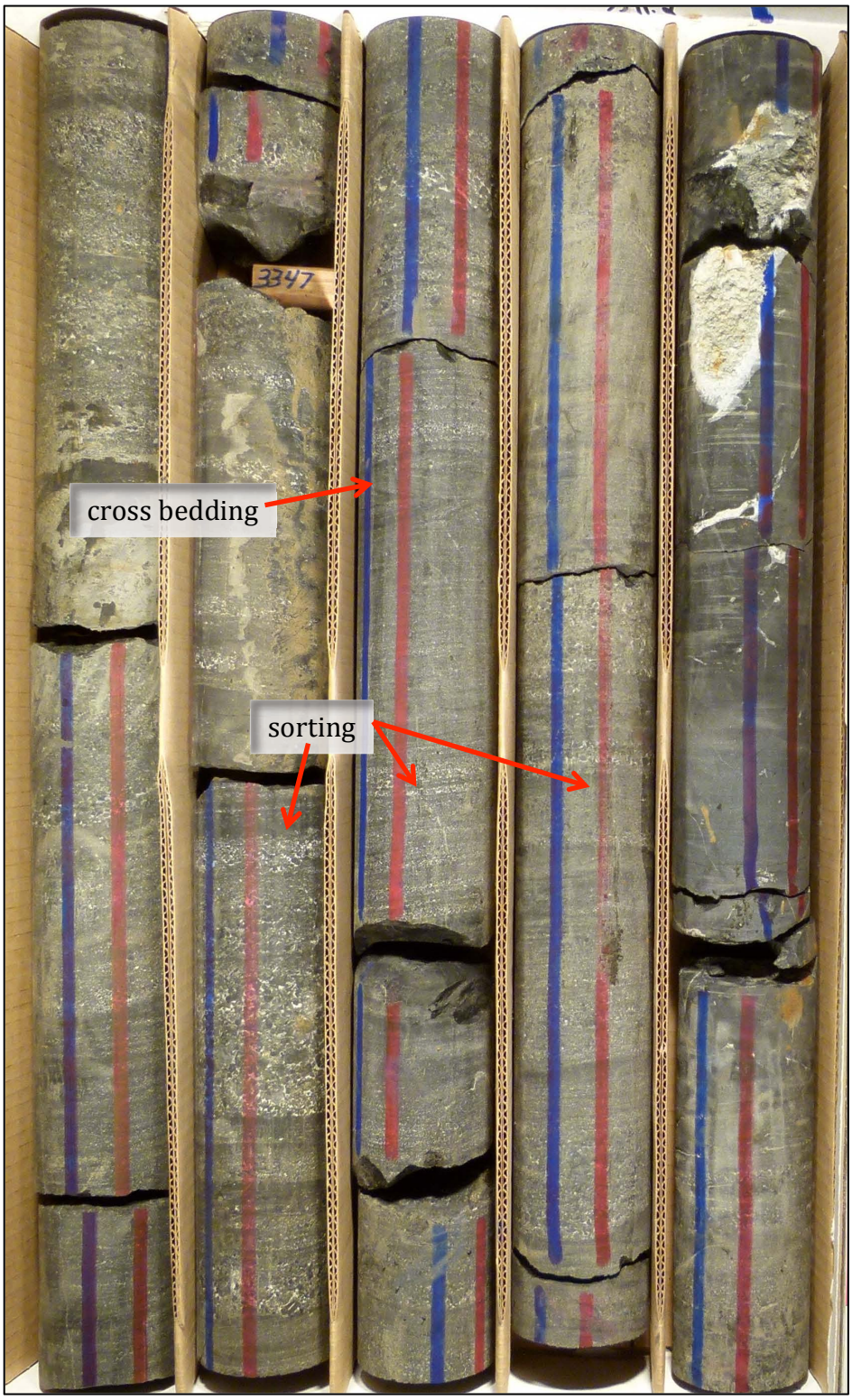

Figure 14. Sedimentary structures in basalt sand. Shown here, a section of core at 1022 m bgs with cross bedding and lamina sorted by grain size.

environment. Core samples are light olive brown, dusky yellow, light olive gray, and dark yellowish brown in dry color. Color varies in fine lamina (Figure 15).

Thin section analysis of the mudstones reveals the mudstones to be composed of calcareous clays (react to HCl) with minimal fine quartz silts (Figures 9D, E, and F and 10F). In thin sections procured from a particularly highly fractured mudstone near the base of Unit 3 (~850 m bgs) (Figures 9D, E, and F) multiple fracture events are observed, and veins of multiple origins intersect and offset each other. As is the case in basalts, sparry calcite is observed as fracture fill (Figures 9 D, E, and F, and 10F). The XRD results show that zeolites and chalcopyrite are also present in these samples.

Secondary Lithology

Two secondary lithologies have been characterized, altered basalt and basalt breccia. These lithologies indicate alteration processes significant to the geothermal system at the MH-2 hole, and therefore necessary to characterize independently of the primary lithologies. While minor in total amount their presence is significant because they may play an important role acting as a seal in a geothermal system.

Altered Basalt

Altered basalts are defined as basalts with a bulk rock composition of >30% alteration minerals. The primary rock is described similarly to the primary basalt, but has undergone a high degree of alteration. They occur in 7 zones (1804.7 - 1795.3 m bgs, 1732.2 - 1724.6 m bgs, 1531.6 – 1517.9 m bgs, 1408.5 – 1331.4 m bgs,

Figure 15. Core box containing mudstone, 829.2 (top right) – 831.2 (bottom left) m bgs. Laminar bedding planes observed, varying in color.

1255.5 – 1244.5 m bgs, 1143.9 – 1116.2 m bgs, and 933.9 – 887.0 m bgs) (Plate 1). Altered zones seem to be coincidental with hyaloclastite deposits and brecciated zones (Plate 1), by either bracketing, or occurring between, or adjacent to those strata.

Basalt Breccia

Brecciated basalts are present in 3 zones 1750 – 1708, 1518 – 1487, and 1383 – 1364 m bgs (Figures 3, 12B, 16, and 17). They are composed of very coarse gravel sized blocky basalt fragments in a matrix of finer angular to sub rounded sand sized shards of basalt and inter growth of calcite, analcime, zeolites, and clay. Vesicles in basalt fragments are filled with clay (Figure 12B and Table 2). Brecciated units in the MH-2 core display fluid assisted critical hydrofracturing, resulting in both volume expansion and volume reduction, under lithostatic load and volatile pressure (Jébrak, 1997; Kirwin, 2006). In some core samples basalt fragments are "floating" in microcrystalline alteration matrix (Figure 17), which indicates rapid mineralization, consistent with an explosive and chaotic event.

Litho-stratigraphy of the MH-2 Borehole

The five litho-stratigraphic units are delineated based on the dominant lithologies and intercalations of subdominant lithologies observed, and inferred depositional setting. These units indicate variability in volcanic, tectonic, and depositional environment. They are numbered 1 – 5 with Unit 1 being the oldest and Unit 5 the youngest.

Figure 16. The hand sample of a brecciated basalt procured from 1383.8 m bgs, and the core box contains core from 1373.4-1376.3 m bgs. The hand sample exhibits angular basalt clasts in host rock groundmass.

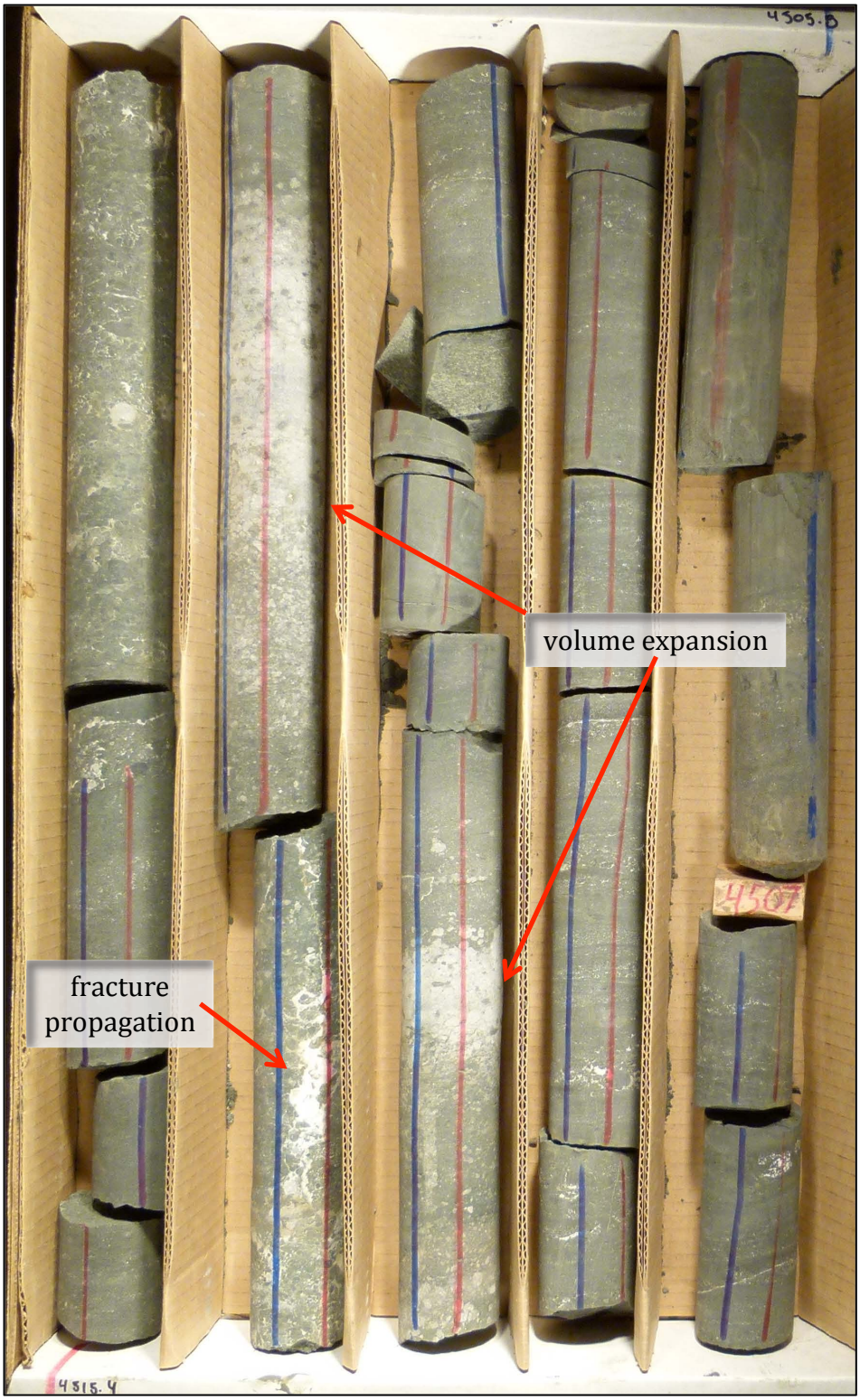

Figure 17. Core box containing brecciated basalt, 1373.4 (top right) – 1376.3 (bottom left) m bgs. Examples of volume expansion, fracture propagation, and rapid secondary mineralization shown.

Unit 1, Subaerial Basalt

The lower 544 m of core (1277 – 1821 (TD) m bgs) is composed primarily of subaerially emplaced basalts, with a thin basalt sandstone at 1732.2 – 1737.4 m bgs (Plate 1). There are 3 zones of breccias and associated surrounding alteration (1708 – 1750, 1487 – 1532, and 1331 – 1409 m bgs) and one localized altered zone (1795 – 1805 m bgs) (Plate 1). The thick basalt flows in this unit are mostly fine grained crystalline with observable plagioclase and olivine phenocrysts, except at the flow margins where vesicles are interspersed in glassy groundmass.

Unit 2, Subaqueous Basalt

Unit 2 (850 – 1277 m bgs) consists of intercalated basalts (unaltered and altered), basalt sandstones, hyaloclastites, and thin mudstone deposits (Plate 1). We define this unit as subaqueous basalt, because water has played an important role in the formation of the lithologies observed. The onset of an aqueous environment is identified at the base of the unit as a series of thin interfingered hyaloclastites, mudstones, basalt flows, and basalt sandstones. Hyaloclastites are a dominant lithology as are fluvial basalt sands and flows. The hyaloclastite deposits are progressively thicker up-section, indicating an increasing persistence and depth of a water body (Plate 1). The middle and upper hyaloclastite deposits are separated by a series of basalt flows and basalt sands (Plate 1). The basalt sands display sedimentary structures indicative of fluvial deposition (Figure 14).

Unit 3, Deep-Water Environment Muds

A decline in the abundance of basaltic rocks marks the base of Unit 3 (553 – 850 m bgs). The unit is composed primarily of a thick package of highly calcareous, clay rich mudstone, indicative of a deep-water depositional environment. A basaltic eruptive event as marked by two individual basalts flows bounding a basalt sandstone segments this unit at 737.6 – 862.0 m bgs.

Unit 4, Siliciclastics

A change in dominant grain size and mineralogy, from calcareous mudstone to siliceous siltstone and sandstone, marks the break between Units 3 and 4 (553 – 213 m bgs). This indicates sourcing of terrigenous siliciclastic materials into the basin. Variability in grain size can be attributed to variability in proximity of the sediment source. Two basalt flows with corresponding basaltic sandstones are described as being present in this unit (518 – 542 m bgs). A mudstone deposit (413 – 436 m bgs) overlies a gravely coarse sandstone deposit (436 – 440 m bgs), possibly indicating changes in lake level during this time.

Unit 5, The Basalt Returns

The siliciclastic deposits are capped by subaerial basalts (161.5 – 213 m bgs). At the base of this unit is a fluvial basalt sandstone deposit (200 – 213 m bgs), which is overlain by a number of basalt flows. These flows are characterized as subaerial and ranging in texture from vesicular and glassy to crystalline. Crystalline zones commonly display large (3 – 5 cm) plagioclase phenocrysts in a sunburst radial pattern (Figure 6).

Wireline Logs

Wireline logs acquired from the MH-2 hole offer an opportunity to correlate the petrophysical properties observed in logs to the examined and described lithologies. Gamma-ray logging was performed from the surface down to 1675 m bgs, the TD at the time of logging. Spectral gamma, sonic velocity, and resistivity logs were acquired in a portion of the open hole below the HQ rods (1167 m bgs), and were also limited to the TD at the time of logging, 1675 m bgs.

Gamma-ray Log

The gamma-ray log is the passive measurement of the radioactivity of the rock as it passes through it (Serra, 1983). Gamma-ray logging of the MH-2 hole shows that main breaks in lithology from volcanic rocks to sedimentary, particularly the lacustrine mud and siltstones, indicated by an increase in measured passive radioactivity in the gamma log (738, 853, and 1214 m bgs)(Plate 1). The lacustrine mud deposits accumulate clay minerals containing radioactive elements and account for the relatively high API readings, as opposed to the basalts, which are depleted of minerals with radioactive isotopes and have very low API signal on the gamma tool log. Where overlap exists between the master and spectral gamma-ray (1167 – 1675 m bgs), we observe proportionate peaks and valleys in contributions from K, U, and Th to the overall gamma profile. At 1213 – 1237 m bgs the gamma log exhibits a large amount of variability indicative of the thin intercalations of mudstones, basalt flows, basalt sandstones, and hyaloclastites in this section, the

mudstones have a high abundance of gamma radioactivity and everything else has low gamma radioactivity.

Sonic Velocity

The velocity profile of the MH-2 hole is a proxy for bulk rock densities and when correlated to the lithology log seems to identify density contrasts between the unaltered basalts (fast) and the other slower velocity rocks (Plate 1). This is most easily observed at contacts between a zone of brecciation and alteration and the surrounding unaltered basalt (1483 – 1529 m bgs), as both Vp and Vs velocity profiles go from relatively fast in the unaltered basalts to relatively slow in the brecciated and altered unit. This is also observed in another altered basalt and basalt breccia unit above (1328 – 1413 m bgs). A similar relationship is observed in density contrasts between basalt (fast) and subaqueous deposits (slow), best shown at the highly variable interval of finely interbedded mudstones, hyaloclastites, basalt sandstones, and basalt flows (1213 – 1277 m bgs). The velocity is not as good as the gamma profiles at delineating the finer scaled changes in lithologies as the interbedded section shows up in the velocity logs as all slow as compared to basalts above and below. The velocity profile through the lacustrine deposits is inverse to the gamma logs higher radioactivity coincides with slower velocities.

Resistivity

The resistivity log, a proxy for water saturation in rocks (Serra, 1983), closely follows the profile of the velocity logs, i.e. unaltered basalts are highly resistive and

everything else has a lower resistivity, albeit at a higher resolution then that of the velocity log (Plate 1). As is the case in the velocity logs, zones of brecciation and alteration (1529 – 1483 and 1413 – 1328 m bgs) have a lower measured resistance then the surrounding unaltered basalts. However, within the unaltered basalts there is variability in the resistivity profile. This is related to variability in basalt flows associated with vascularity and crystallinity and possibly flow composition.

DISCUSSION AND INTERPRETATIONS

The litho-stratigraphy characterized in the MH-2 core indicates a dynamic depositional and tectonic environment and history. Here we merge the 5 stratigraphic units into accepted geologic models of the Western Snake River Plain.

Secondary lithologies, while not indicative of the geologic history of those rocks, are significant to the geothermal system at the MH-2 drill site. As identified in the sonic velocity and resistivity logs, relatively lower density brecciated and altered zones with higher abundances of hydrous mineral phases may be acting as hydrothermal fluid seal. They may also indicate previous depths to the top of flowing thermal waters.

Shervais et al (2016) identified three candidate play types in the Snake River Plain to examine with further work to determine if there are exploitable geothermal resources. One of these is the mid-crustal basalt sill complex, in which the MH-2 drillhole lies at the southern margin. This result indicates that geologic analyses of the MH-2 hole serves to estimate how it fits into the regional geothermal system.

Geologic Interpretation

The five litho-stratigraphic units identified by dominant lithology, also distinctly capture significant changes in depositional environment and tectonic setting (Plate 1).

Unit 1 consists of sub-aerially emplaced basalt flows (bottom of the core to 1277 m bgs) and lacks any evidence of fluvial or lacustrine influence. This may indicate the early history of rifting in the WSRP. Wood and Clemens (2002) put the

onset of major faulting at the margins of the WSRP at 11 Ma. They also infer that much of the area may have been uplands during the period of silicic volcanism (12-10 Ma), as rhyolite does not occur in deep wells in the northwestern potions of the WSRP although domes are proximal.

The subaqueous basalts (hyaloclastites and basalt sandstones) of Unit 2 (1277 m bgs to 887 m bgs) indicate a stronger influence of lakes and rivers than in Unit 1. Hyaloclastites, as described in the results, indicate rapid quenching and proximal water sources or sub-aqueous emplacement, as a flow either entered a water body or erupted into it. The progressively thicker deposits of these lithologies upsection in Unit 2 indicates that the presence of water was increasingly common and deeper with time, perhaps by the formation of a well-established fluvial system and later a lake. The fine interfingering of lacustrine mudstones, fluvial basalt sands, hyaloclastites, and subaerial basalts at the base of this unit is interpreted as the introduction of fluvial activity in the area with intermittent damming by basalt flows, forming relatively short-lived lakes. The lakes later became more permanent as the basin continued to drop. The landscape at this time is an active rift environment with lakes, interconnected at times by a river system, much like that of the modern-day East-African rift lakes and rivers system.

Units 3 (551 – 887 m bgs) and 4 (215 – 551 m bgs) are typified by deep-water sedimentary deposits, by first lime mud deposition and then terrigenous clastic sedimentation. They likely represent the history of the Plio-Pleistocene Lake Idaho. This was a period of diminished basaltic volcanism in the area. They are segmented by a transition in dominant grain size and mineralogy from calcareous

and clay rich muds in Unit 3 to quartzofeldspathic silts and sands in Unit 4. Wood and Clemens (2002) describe an overflow event, in which Lake Idaho rose to it's highest level and spilled over into ancestral Hells Canyon. A spillover of Lake Idaho and formation of Hells Canyon was first proposed by Wheeler and Cook (1954). The timing is poorly constrained to be between 1.67 and 6.4 Ma, based on magnetic polarity in transgressive sequence shoreline sediments and $Ar^{40/39}$ dating of basalt overlying sediments and gravels near the outlet (Wood and Clemens, 2002). Fossil and fauna analysis place the formation of Hells Canyon to between 3 and 4 Ma (Repenning et al., 1995). As the lake level dropped shorelines were eroded into and deltas prograded northwest or basinward (Wood, 1994), supplying the basin with coarser sediments than previously, interpreted here as being represented in the MH-2 core as the boundary between Units 3 and 4. The basin filled with sediment from east to west and ended at the outlet at 1.67 Ma.

Unit 5 is a cap of the youngest basalts. Geochemical dating of these basalts indicates that a resurgence of volcanism began as early as 2.2 Ma (Shervais et al., 2002, 2005). The base of Unit 5 is a package of basaltic sands, indicating the earliest basalts may have erupted in proximity of a water body. Sediment structures observed in these basalt sandstones indicate they were fluvially reworked by the ancestral Snake River, as it was established in place at this time (Wheeler and Cook, 1954).

Overall the MH2 core represents a sequence of basaltic eruptions interspersed with fluvial hiatus, the development of lakes, and Plio-Pleistocene basalt volcanism.

Secondary Lithology and MH-2 Geothermal System Implications

Brecciation of primary basalts observed in the MH-2 core is likely a result of boiling at depth. Atkinson (2015) determined that hydrothermal waters once reached temperatures of at least 260 °C, and possibly as hot as 370 °C, hot enough to boil at pressures between 4.7 MPa and 21 MPa (well within pressures expected at these depths), based on fluid inclusion analysis.

The site of artesian flowing water found during drilling is located at the bottom of the deepest brecciated zone, which indicates that this breccia, and the alteration mineralization that supports it, may be acting as a seal. This is a notion that is echoed by Kessler (2014), who theorizes, based on his uniaxial compressive strength experiments of core samples and fracture density counts in the core, that highly altered zones deform ductiley and form seals; as opposed to the more brittle fresh basalt that when fractured, form connected pathways that act as porosity and permeability in the geothermal reservoir (Figure 24). The two shallower zones of brecciation may indicate previous locations of the geothermal fluid. The occurrence of highly thermally altered basalts in close stratigraphic proximity to breccias would support this theory.

Chalcopyrite is identified in XRD analysis at depths of 758, 849, and 1731 m bgs. Under geothermal conditions, chalcopyrite forms at temperatures of 200 – 300 °C (Zhao et al., 2014), indicating that temperatures were once higher at much shallower depths than the current location of the thermal zone. The results of Atkinson (2015) indicating a decrease in temperature at the thermal zone, the

possibility of a retreat of the geothermal system from previously shallower depths to its current location, and the temperature of mineralization of chalcopyrite and its location in the core indicates the system is cooling. Geochronology of alteration phases in the core could constrain the timing and rate of cooling.

Play Fairway Analysis and Regional Geothermal Model

The DOE funded geothermal evaluation of the Snake River Plain adopted an oil and gas risk assessment called Play Fairway Analysis (PFA) (Shell Exploration and Production, 2013). In a PFA assessment, a play type, or type of resource target, is delineated into a fairway of prospects. The USU SRP assessment identified 3 play types in the SRP, 2 relatively well known geothermal resource play types, Basin-and-Range and silicic domes, and a third type proposed by the team being the SRP mid-crustal basalt sill complex (Shervais et al., 2016). I discuss the SRP basalt sill complex play type here, as the MH-2 well lies within this regime and may represent the discovery well for this play type. For each play type a series of maps termed critical risk segment maps (CRS) were constructed from data layers, which map both the spatial distribution of a critical element and the data confidence of that element (DeAngelo et al., 2016). For example, an element identified as critically important is complex fault systems and fault intersections, as these may act as fluid flow pathways for geothermal fluid to travel along. A map of surface faults was constructed (Figure 18); areas with a high density of fault intersections are given a favorable score and then that map is evaluated for confidence in the data, the criteria for which is the resolution at which that map was made, higher resolution

gets a higher score (Figure 21). For this project I assembled a database of relevant publically available data, and mapped those data in a series of ArcGIS database layers (see Appendix B for details). Data sets used to create this database include mapped surface faults, location and temperature of hot springs, location, age, and chemical composition of volcanic vents, areal extent and the thickness of cold water aquifer, surface geology, and cadastral were collated, mapped, and layered to identify correlations of significance to the geothermal exploration project (Figures 18, 19, 20, and 22). Those data layers are evaluated for confidence in the data and rated for quality of the feature with regards to the geothermal system, resulting in a CRS map. These scored CRS maps are then layered to form a composite common risk segment (CCRS) map. The CCRS map is a map indicating the highest confidence fairways for this play type.

The Mountain Home area is one of at least 5 prospects identified in the WSRP of the mid-crustal sill complex play type (Figure 23). A selection of CRS maps used to identify these prospects in the CCRS are the permeability, heat source, and seal risk segments. Development of these CRS maps were beyond the scope of my contribution, but are significant to the discussion of the geology of the MH-2 hole and the presence of thermal water within. Permeability is derived from the density of mapped faults and deep gravity lineaments dilatation and slip data layers. The heat source is a combination of density of volcanic vents weighted by age and size, and heat flow calculated from well temperature logs. The seal CRS map depicts the presence of paleo-lake sediments weighted by thickness and the base of the shallow water aquifer (DeAngelo et al., 2016). The MH-2 drill site is located on the northern

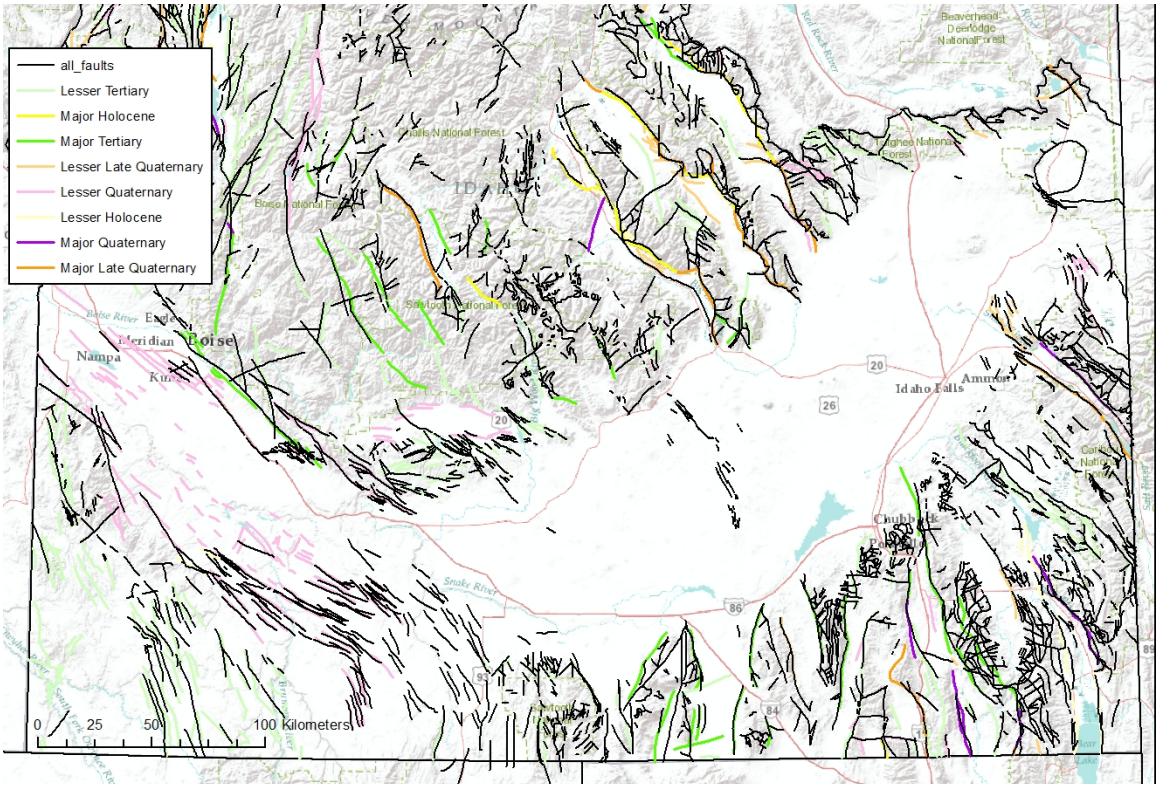

Figure 18. Mapped surface faults in southern Idaho.

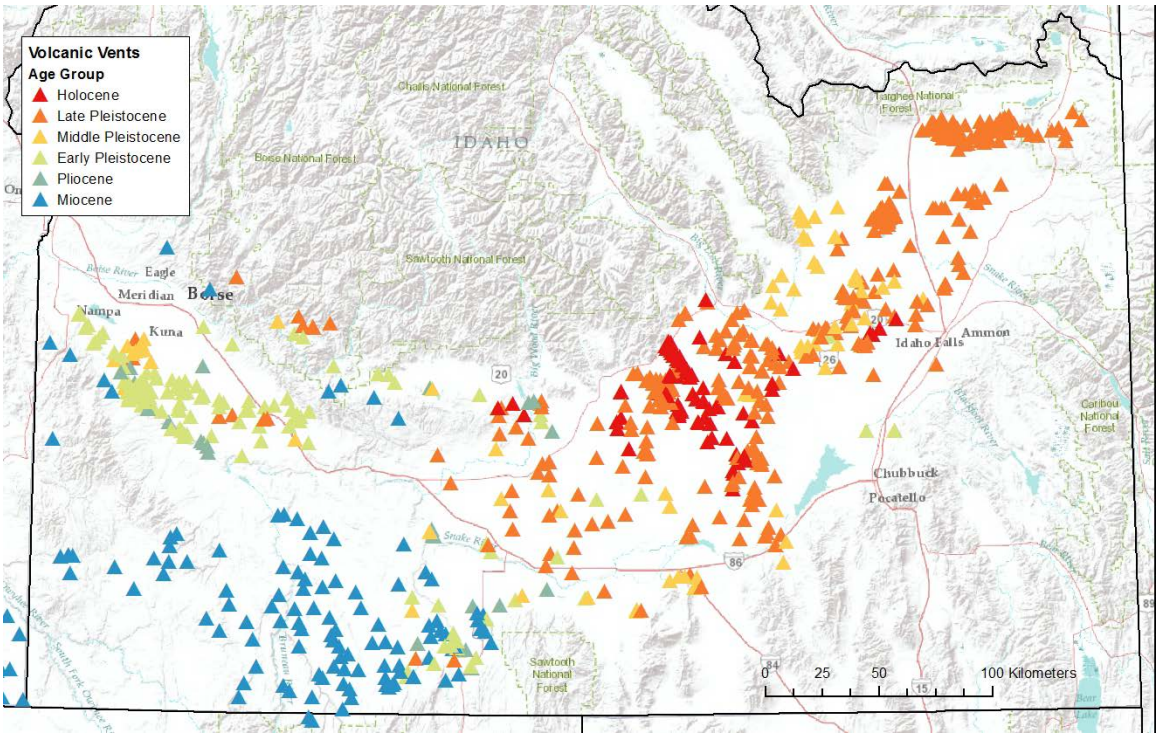

Figure 19. Volcanic vents of the Snake River Plain and surrounding area mapped by age.

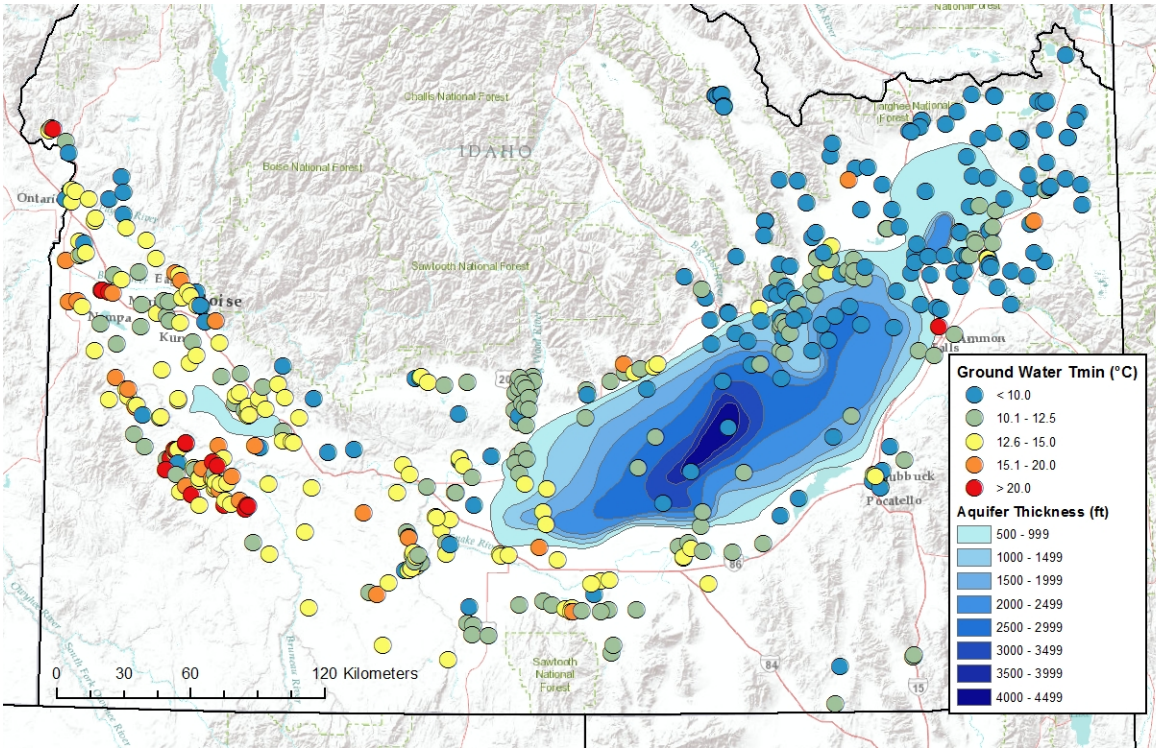

Figure 20. The Snake River Plain aquifer thickness and ground water temperatures.

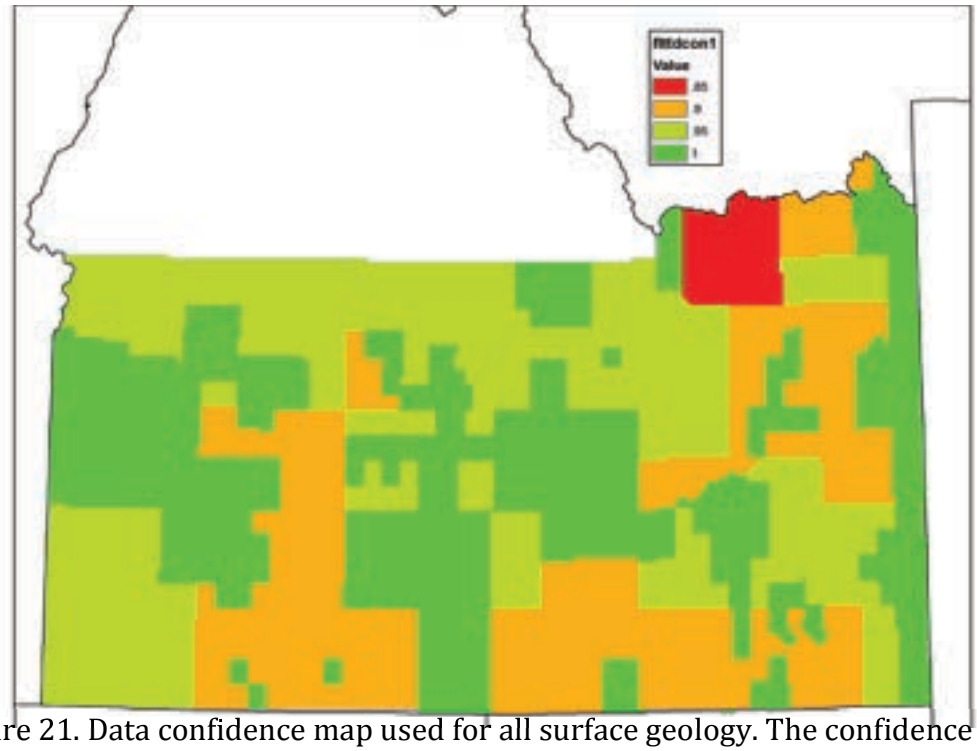

Figure 21. Data confidence map used for all surface geology. The confidence score is based on the scale at which the geologic maps were constructed: red=>1:250,000, Orange=1:100,000 – 1:250,000, light green=1:50,000 – 1:100,000, and dark green=≤1:50,000

edge of a fairway, located in a larger cluster of fairways that trend NW-SE (Figure 23), parallel to the trend of permeability and sub-parallel to the nearly E-W trend of volcanic vents. Bostic 1a falls within the fairway that occurs to the north of MH-2, suggesting that these systems of the same play type and orientation, have discrete properties that limit areal extent.

A comparison of the MH-2, MH-1, and Bostic-1A lithology logs (Figures 25 and 26) indicates key features of the geothermal system may not be continuous. Many subsurface faults exist (Figure 24) (Lewis and Stone, 1988; Arney et al., 1984; Shervais et al., 2002; Kessler, 2014) and offsets between reservoirs and seals may

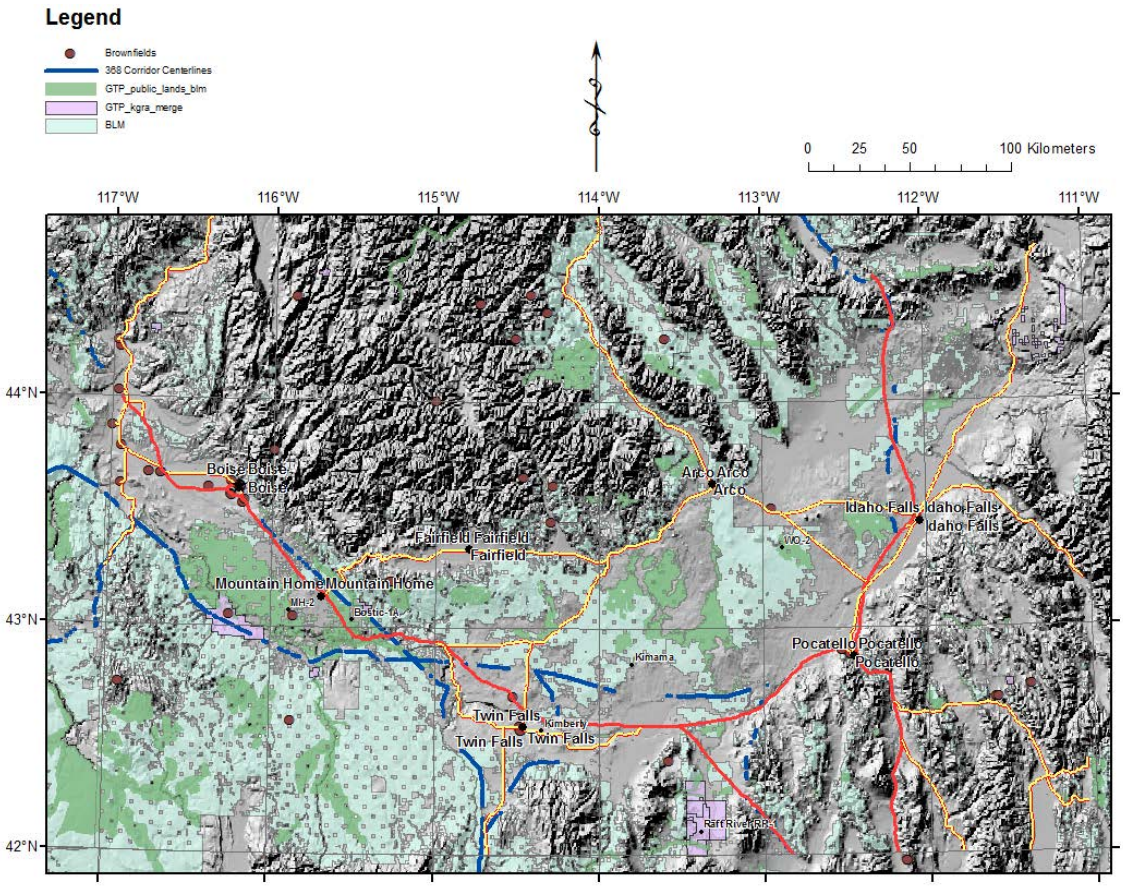

Figure 22. A map of potentially drillable areas in southern Idaho based on land management type. From Shervais et al. (2016).

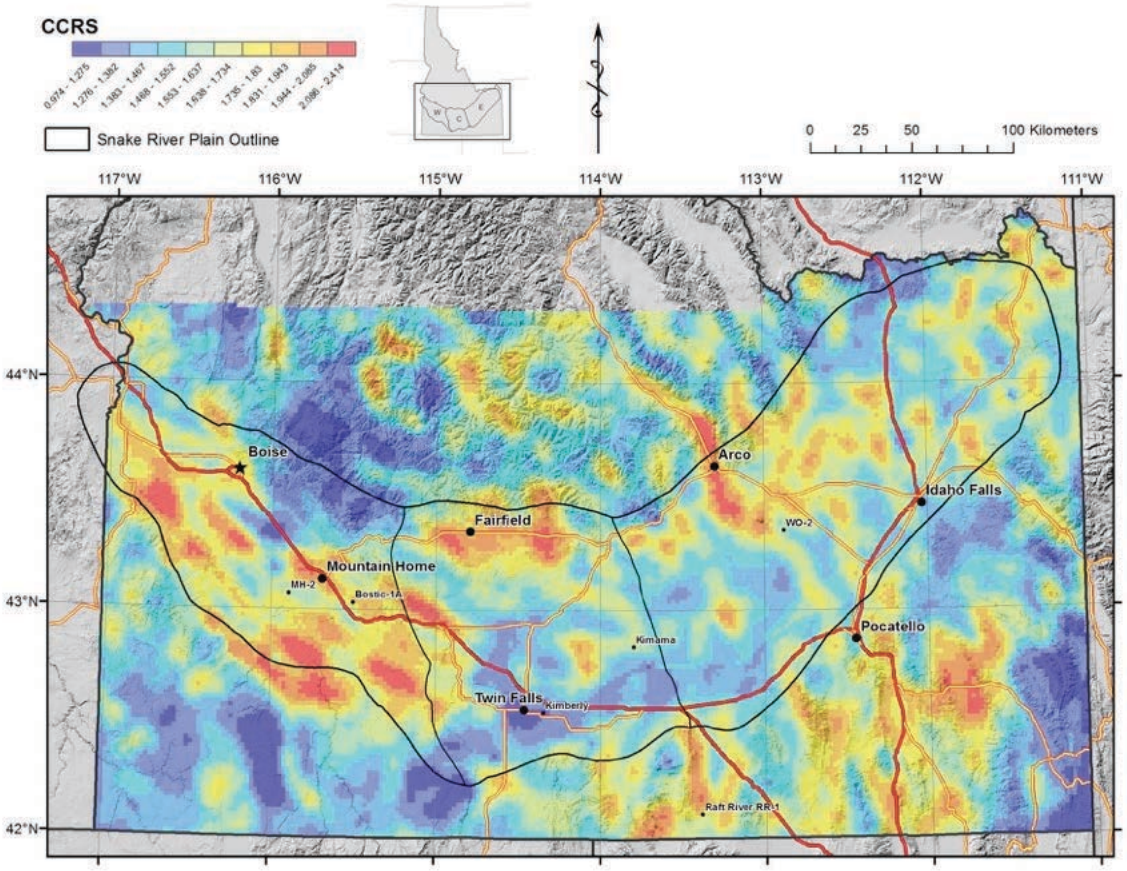

Figure 23. A composite common risk segment map of the Snake River Plain, adapted from DeAngelo, 2016. Heat source, permeability, and seal risk segment maps were layered to form this composite. Red indicates the highest probability that these elements exist and overlap to form a geothermal resource system.

exist as well, in a lateral extent as small as 4.6 km (distance between MH-2 and MH-1). A fault offset may be responsible for nearly 300 m of missing lacustrine deposits in the MH-1 hole, as compared with MH-2 (Figures 25 and 26). This would require at least 300 m of vertical separation, assuming an idealized fault geometry where the strike is parallel to the horizontal plane projection of separation and a dip of 60°,

this requires ~350 m of strike-perpendicular slip. Assuming the mantling of basalts are unfaulted, the slip rate on these proposed intrabasinal normal faults would had to have been at least a modest 0.2 mm/yr. This interpretation is consistent with that of unpublished work by Shervais, where he describes the mid crustal gravity anomaly to be an intrabasinal structural horst, with en echelon bounding normal faults. The fault systems on either side of the horst may provide the permeability for the geothermal system. The structure also effectively segments the two fairways that the MH-2 site and Bostic 1a site occur within (Figure 27).

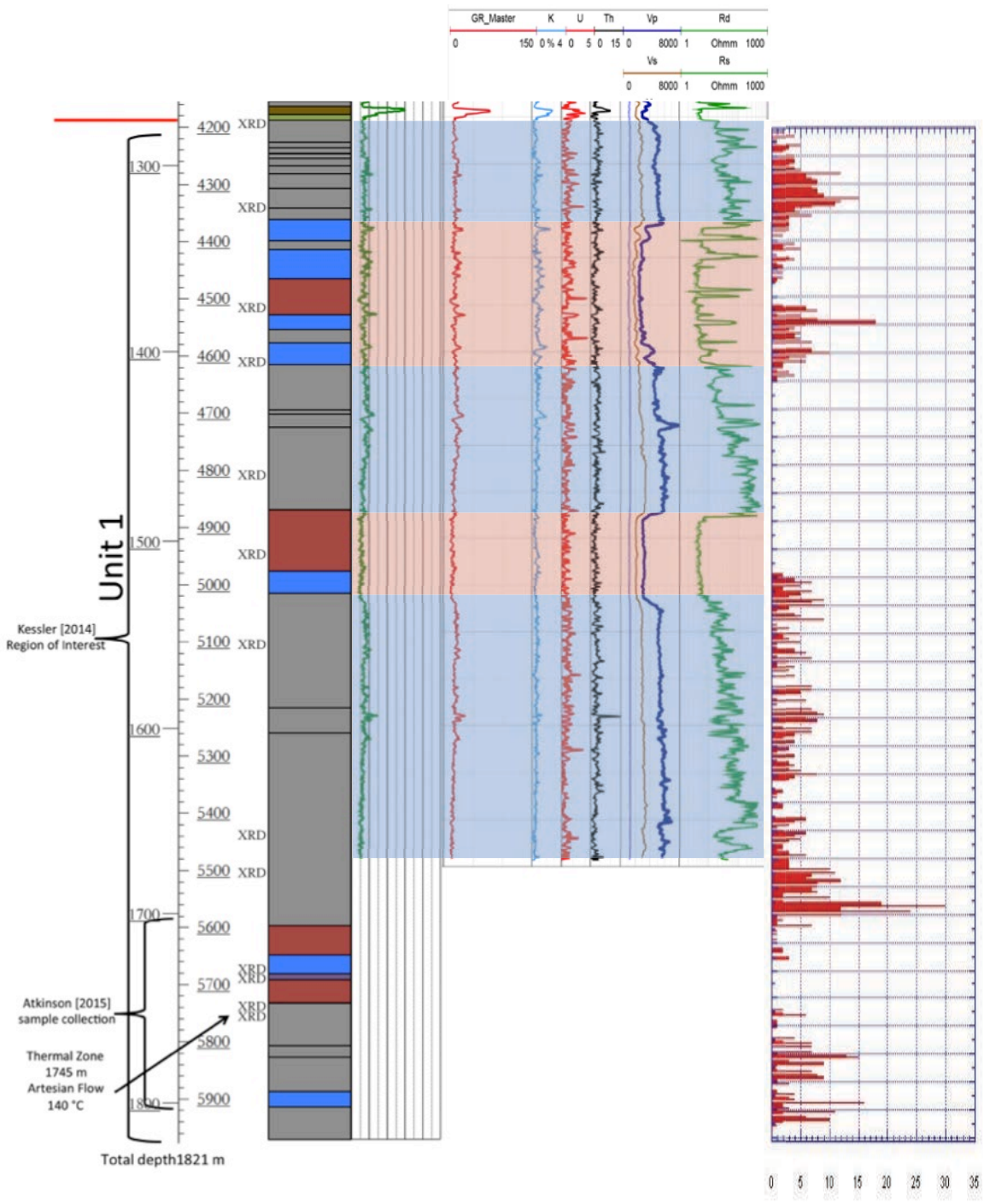

Figure 24. Litho-stratigraphic unit 1 and corresponding logs merged with fracture density counts in this section of core from Kessler (2014). Higher fracture densities seem to coincide with zones of unaltered basalt. Wireline logs are color annotated to indicate major breaks in sonic and resistivity logs.

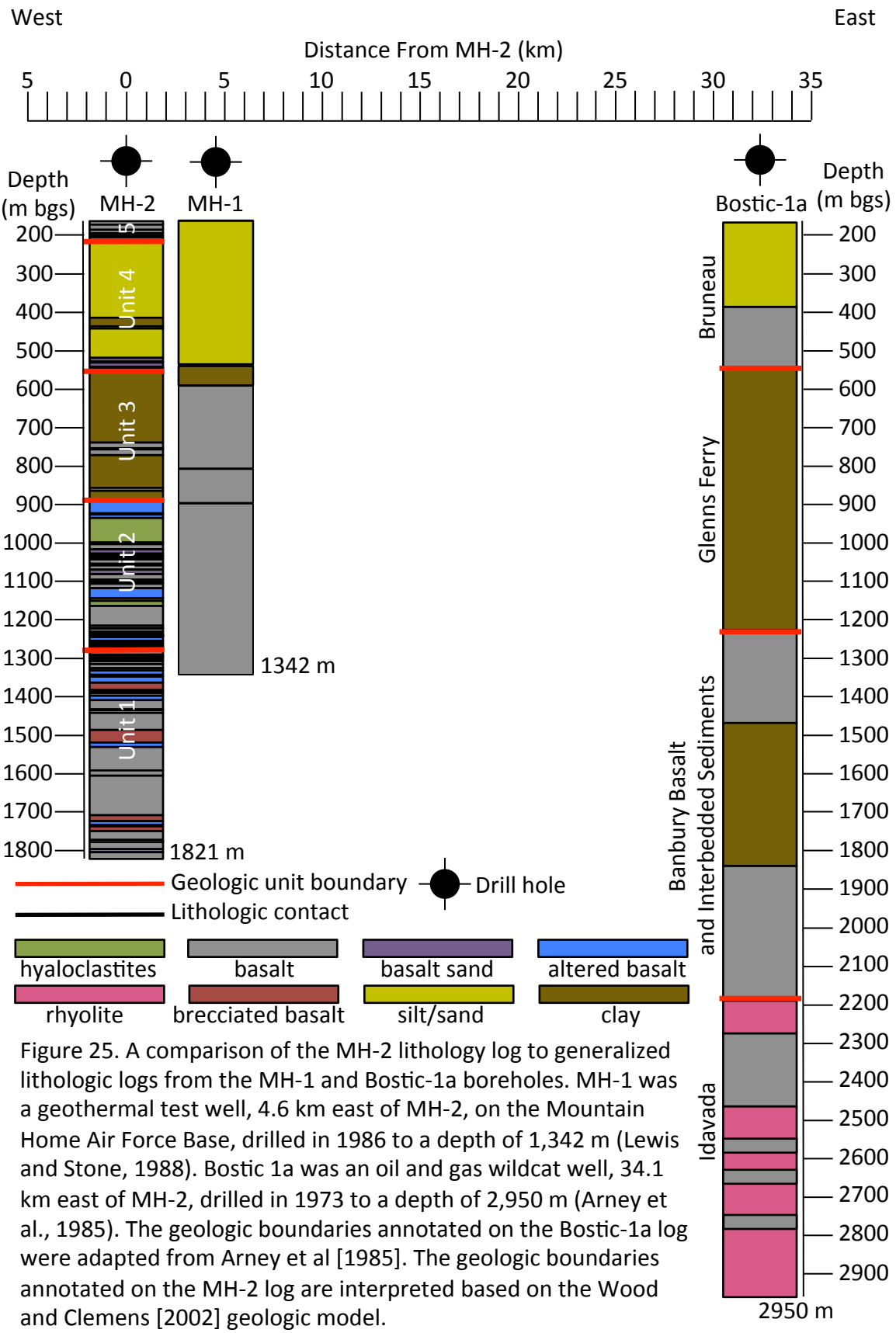

Figure 25. A comparison of the MH-2 lithology log to generalized lithologic logs from the MH-1 and Bostic-1a boreholes. MH-1 was a geothermal test well, 4.6 km east of MH-2, on the Mountain Home Air Force Base, drilled in 1986 to a depth of 1,342 m (Lewis and Stone, 1988). Bostic 1a was an oil and gas wildcat well, 34.1 km east of MH-2, drilled in 1973 to a depth of 2,950 m (Arney et al., 1985). The geologic boundaries annotated on the Bostic-1a log were adapted from Arney et al [1985]. The geologic boundaries annotated on the MH-2 log are interpreted based on the Wood and Clemens [2002] geologic model.

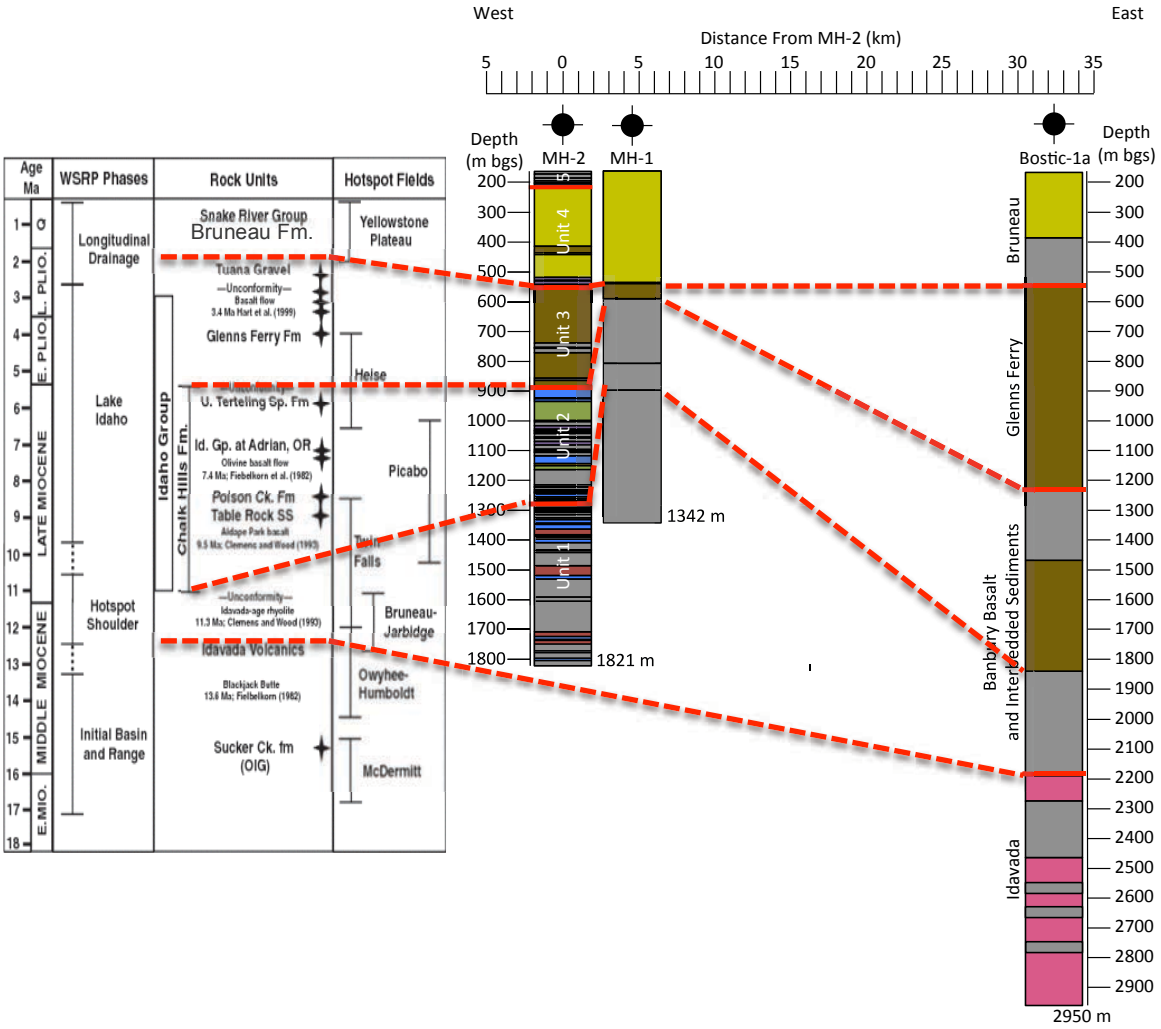

Figure 26. Plausible stratigraphic correlations between MH-2, MH-1, and Bostic-1A are shown. Geochronologic constraint is necessary to validate or disprove these correlations. Stratigraphy modified from Beraneck et al. (2006).

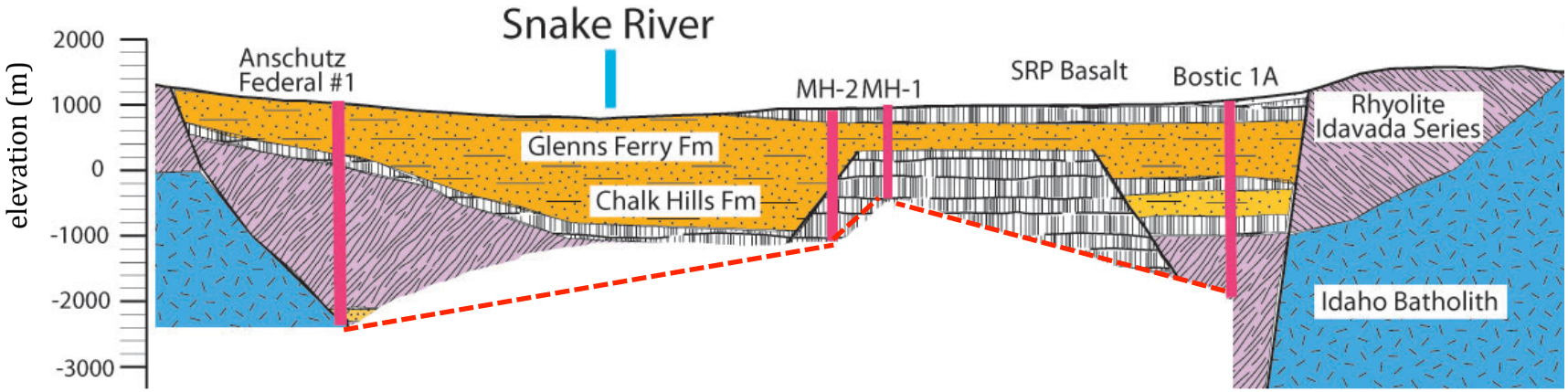

Figure 27. Subsurface cross-sectional model based on gravity anomaly, drill hole, seismic data, and geologic interpretation. Modified from unpublished work by Shervais. The proposed horst explains the missing stratigraphy in the MH-1 core as compared with MH-2, and the segmented nature of the 2 parallel fairways following the trend of the faults bounding the horst.

CONCLUSIONS

The MH-2 core acquired from the Mountain Home Air Force Base, in the western Snake River Plain, Idaho, represents the geologic history of an intracontinental rift basin that formed prior to and as a result of the passing Yellowstone Hot Spot over the past 11 million years. The deepest lithologies in the core are basalts that first erupted subaerially (litho-stratigraphic Unit 1) and later subaqueously as a basin formed and formed a system of lakes connected by rivers (litho-stratigraphic Unit 2). As volcanic activity diminished and lake levels continued to rise, a thick package of lacustrine sediments was deposited as lime muds (litho-stratigraphic Unit 3). The lake eventually rose to a level where it catastrophically spilled over into ancestral Hells Canyon, and cut down to a new base level. As the lake drained, shorelines were eroded into and deltas prograded supplying terrigenous siliciclastic silts and sands to the basin (litho-stratigraphic Unit 4). These sediments were then covered by a resurgence of basaltic volcanism deposited first subaqueously and then erupting to the surface (litho-stratigraphic Unit 5).

An overprint of faults, fractures, and breccias is represented in core. Brecciation is a result of boiling at depth. Alteration minerals, zeolites, calcite, chalcopyrite, and analcime, indicate paleo-hydrothermal fluid flow. In the zone where artesian flowing thermal water was encountered, plagioclase has been remineralized from labradorite type to albite type. Zones of higher permeability, either primary such as in hyaloclastites, or secondary as in fractured zones, have a higher incidence of alteration, and may have once been reservoirs for hydrothermal

fluid. The most common secondary mineral type, zeolites, exists as fracture and void fill, as does calcite, which is common in voids such as vesicles and vugs. High abundances of clay are present and deposited as degradation of primary minerals and glasses in vesicle rinds and groundmass, and along fluid flow pathways and fractures. XRD results indicate that all clays are smectite variety, accept for in the thermal zone, where kaolinite was detected. Conspicuously missing from XRD analysis is the presence of quartz, which may be a result of the high alkalinity of the hydrothermal fluid. Indications that the geothermal zone was located at shallower depths than its current location and mineralization paleothermometry indicate the geothermal system is cooling, but the rate of cooling is not constrained.

Systematically identified in a Play Fairway risk assessment, the Western Snake River Plain is highly prospective as a geothermal energy natural resource, with multiple fairways with the potential to be developed. Combining the finer scaled analysis of the MH-2 core aids in identifying the lithology that the geothermal system is comprised of and revealed that broader regional scale controls differ from the finer scale core controls. A zone of brecciation with secondary mineralization, at the interface of the geothermal zone, may be acting as geothermal fluid seal at MH-2. The broader scale heat seal may be the lacustrine package of sediments. The finer scale core level descriptions are useful at identifying the system at a single point, core-to-core correlations reveal that areal extent of these systems are not continuous. Basin scale modeling reveals that continuity is controlled by intrabasinal normal faults, indicating the importance of understanding the subsurface structure in detail. The regional scale control on the extent of these

fairways seems to be explained well by the model presented by the interpretation of the subsurface data. It will take further exploration to prove this model.

REFERENCES CITED

Armstrong, J.C., Breckenridge, R.P., Nielson, D.L., Shervais, J.W., and Wood, T.R., 2013, Mountain Home Air Force Base, Idaho Geothermal Resource Assessment and Future Recommendations: Idaho National Laboratory (INL) No. INL/EXT-12-26319.

Arney, B.H., Garnder, J.N., and Belluomini, S.G., 1984, Petrographic Analysis and Correlation of Volcanic Rocks in Bostic 1-A Well near Mountain Home, Idaho: Los Alamos National Laboratory Report, v. LA-9966-HDR.

Arney, B.H., and Goff, F., 1982, Evaluation of the hot-dry-rock geothermal potential of an area near Mountain Home, Idaho: LA-9365-HDR, 5350339.

Atkinson, T., 2015, Geochemical Characterization of the Mountain Home Geothermal System [M.S.]: Utah State University, 104 p.

Beranek, L.P., Link, P.K., and Fanning, C.M., 2006, Miocene to Holocene landscape evolution of the western Snake River Plain region, Idaho: Using the SHRIMP detrital zircon provenance record to track eastward migration of the Yellowstone hotspot: Geological Society of America Bulletin, v. 118, p. 1027–1050, doi: 10.1130/B25896.1.

Blackwell, D.D., and Richards, M., 2004, Geothermal Map of North America: American Association of Petroleum Geologists.

Blackwell, D.D., Richards, M.C., Frone, Z.S., Williams, M.A., Ruzo, A.A., and Dingwall, R.K., 2011, Temperature at depth maps for the conterminous US and geothermal resource estimates: Geothermal Resources Council Transactions, v. 35, p. 1545–1550.

Bonnichsen, B., and Godchaux, M.M., 2002, Late Miocene, Pliocene, and Pleistocene geology of southwestern Idaho with emphasis on basalts in the Bruneau-Jarbidge, Twin Falls, and western Snake River Plain regions.: Tectonic and Magmatic Evolution of the Snake River Plain Volcanic Province: Idaho Geological Survey Bulletin 30, p. 233–312.

Breckenridge, R.P., Nielson, D., Shervais, J.W., and Wood, T.R., 2012, Exploration and Resource Assessment at Mountain Home Air Force Base, Idaho, Using an Integrated Team Approach: Geothermal Resources Council Transactions, v. 36, p. 615–619.

DeAngelo, J., Shervais, J.W., Glen, J.M., Nielson, D.L., Garg, S.K., Dobson, P., Gasperikova, E., Sonnenthal, E., Visser, C., Liberty, L.M., Siler, D., Evans, J.P., and Santellances, S., 2016, GIS Methodology for Play Fairway Analysis:

Example from the Snake River Plain Volcanic Province, *in* 41st Workshop on Geothermal Reservoir Engineering, Stanford University, Stanford, CA, p. 10.

Delahunty, C., Nielson, D.L., and Shervais, J.W., 2012, Deep core drilling of three slim geothermal holes, Snake River Plain, Idaho, *in* p. 641–648.

Freeman, T.G., 2013, Evaluation of the Geothermal Potential of the Snake River Plain, Idaho, Based on Three Exploration Wells [M.S.]: Utah State University, 90 p.

Garg, S.K., Nielson, D.L., Shervais, J.W., and Sonnenthal, E., 2016, Thermal modeling of the Mountain Home Geothermal Area, *in* 41st Workshop on Geothermal Reservoir Engineering, Stanford University, Stanford, CA.

Glen, J.M.G., and Ponce, D.A., 2002, Large-scale fractures related to inception of the Yellowstone hotspot: Geology, v. 30, p. 647, doi: 10.1130/0091-7613(2002)030<0647:LSFRTI>2.0.CO;2.

Harðarson, B.S., 2014, Geothermal exploration of the Hengill high-temperature field: Short Course IX on Exploration for Geothermal Resources, p. 9, doi: 001374011.

Jébrak, M., 1997, Hydrothermal breccias in vein-type ore deposits: A review of mechanisms, morphology and size distribution: Ore Geology Reviews, v. 12, p. 111–134, doi: 10.1016/S0169-1368(97)00009-7.

Katherine, L., 1987, Weathering of basalt: formation of iddingsite.: Clays and Clay Minerals, v. 35, p. 418 – 428.

Kessler, J.A., 2014, In-situ stress and geology of the MH-2 Borehole, Mountain Home, Idaho, USA: Implications for Geothermal Exploration from Geomechanics [Dissertation]: Utah State University, 160 p.

Kimmel, P.G., 1982, Stratigraphy, age, and tectonic setting of the Miocene-Pliocene lacustrine sediments of the western Snake River Plain, Oregon and Idaho.: Cenozoic geology of Idaho: Idaho Bureau of Mines and Geology Bulletin, v. 26, p. 559–578.

Kinslow, R., Hass, B., Maddi, P., and Bakane, P., 2012, DEVELOPMENT OVERVIEW OF GEOTHERMAL RESOURCES IN KILAUEA EAST RIFT ZONE: Geothermal Academy, v. 9.

Kirwin, D.J., 2006, Hydrothermal Breccias Textures, Process and Mineralisation:.

Kucks, 1999, Bouguer gravity anomaly data grid for the conterminous US: U.S. Geological Survey, v. National geophysical data grids; gamma- ray, gravity, magnetic and topographic data for the conterminous United States.

Kuntz, M.A., Champion, D., Spiker, E., Lefebvre, R., and McBroome, L., 1983, The Great Rift and the Evolution of the Craters of the Moon Lava Field, Idaho: Bonnichsen, B. and Breckenridge, R.M., eds., Cenozoic Geology of Idaho, v. Idaho Bureau of Mines and Geology Bulletin 26, p. 423 – 438.

Leeman, W.P., 1989, Origin and development of the Snake River Plain (SRP)—An overview, *in* Smith, R.P., Downs, W.F., Christiansen, R.L., Hacket, W.R., Morgan, L.M., Leeman, W.P., and Bonnichsen, B. eds., Snake River Plain-Yellowstone Volcanic Province: Jackson, Wyoming to Boise, Idaho July 21–29, 1989, Washington, D. C., American Geophysical Union, p. 4–12.

Lewis, R.E., and Stone, M.A.J., 1988, Geohydrologic data from a 4,403-foot geothermal test hole, Mountain Home Air Force Base, Elmore County, Idaho: U.S. Geological Survey Open-File Report 88-166, 30 p.

Link, P.K., and Phoenix, E.C., 1996, Rocks Rails & Trails: Idaho Museum of Natuaral History, 194 p.

Malde, H.E., and Powers, H.A., 1962, Upper Cenozoic Stratigraphy of Western Snake River Plain, Idaho: Geological Society of America Bulletin, v. 73, p. 1197, doi: 10.1130/0016-7606(1962)73[1197:UCSOWS]2.0.CO;2.

McIntyre, D.H., 1979, Preliminary description of Anschutz Federal No 1 drill hole, Owyhee County Idaho: U.S. Geological Survey Open- File Report 79-651, 15 p.

Minitti, M.E., Weitz, C.M., Lane, M.D., and Bishop, J.L., 2007, Morphology, chemistry, and spectral properties of Hawaiian rock coatings and implications for Mars: Journal of Geophysical Research, v. 112, doi: 10.1029/2006JE002839.

Nielson, D.L., and Shervais, J.W., 2014, Conceptual model of Snake River Plain geothermal systems:, *in* Thirty-Ninth Workshop on Geothermal Reservoir Engineering, Stanford University, Stanford, CA.

Nielson, D.L., Shervais, J.W., Evans, J.P., Liberty, L.M., Garg, S.K., Glen, J.M., Visser, C., Dobson, P., Gasperikova, E., and Sonnenthal, E., 2015, Geothermal Play Fairway Analysis of the Snake River Plain, Idaho, *in* Fortieth Workshop on Geothermal Reservoir Engineering, Stanford University, Stanford, CA.

Pierce, K.L., and Morgan, L.A., 1992, Chapter 1: The track of the Yellowstone hot spot: Volcanism, faulting, and uplift, *in* Geological Society of America Memoirs, Geological Society of America, p. 1–54.

Repenning, C.A., Weasma, T.R., and Scott, G.R., 1995, The early Pleistocene (latest Blancan-earliest Irvingtonian) Froman Ferry fauna and history of the Glenns Ferry Formation, southwestern Idaho: Bulletin USGS Numbered Series 2105.

Self, S., Keszthelyi, L., and Thordarson, T., 1998, THE IMPORTANCE OF PĀHOEHOE: Annual Review of Earth and Planetary Sciences, v. 26, p. 81–110, doi: 10.1146/annurev.earth.26.1.81.

Serra, O.E., 1983, Fundamentals of well-log interpretation: Elsevier Science Pub. Co., Inc.,New York, NY.

Shell Exploration and Production, 2013, Play Based Exploration: a guide for AAPG's Imperial Barrel Award Participants, *in* Graphics Media and Publishing Services (GMP), Rijswijk, Netherlands.

Shervais, J.W., 2014, The Snake River Geothermal Drilling Project: Innovative Approaches the Geothermal Exploration: Utah State University Final Project Report DE-EE 0002848.

Shervais, J.W., Evans, J.P., Christiansen, E.H., Schmitt, D.R., Liberty, L.M., Blackwell, D.D., and Glen, J.M., 2011, Hotspot: The Snake River Geothermal Drilling Project — An Overview: Geothermal Resources Council Transactions, v. 35, p. 995–1003.

Shervais, J.W., Evans, J.P., Schmitt, D.R., Christiansen, E.H., and Prokopenko, A., 2014, Drilling Into the Track of the Yellowstone Hot Spot: Eos, Transactions American Geophysical Union, v. 95, p. 85–86, doi: 10.1002/2014EO100001.

Shervais, J.W., Glen, J.M., Liberty, L.M., Dobson, P., and Gasperikova, E., 2015, Snake River Plain Play Fairway Analysis–Phase 1 Report: Geothermal Resources Council Transactions, v. 39.

Shervais, J.W., Glen, J.M., Nielson, D.L., Garg, S.K., Dobson, P., Gasperikova, E., Sonnenthal, E., Visser, C., Liberty, L.M., DeAngelo, J., Siler, D., Varriale, J.A., and Evans, J.P., 2016, Play Fairway Analysis of the Snake River Plain: Phase 1, *in* Proceedings, 41st Workshop on Geothermal Reservoir Engineering, Stanford University, Stanford, CA.

Shervais, J.W., Kauffman, J.D., Gillerman, V.S., Othberg, K.L., Vetter, S.K., Hobson, V.R., Zarnetske, M., Cooke, M.F., Matthews, S.H., and Hanan, B.B., 2005, Basaltic volcanism of the central and western Snake River Plain: A guide to field relations between Twin Falls and Mountain Home, Idaho, *in* GSA Field Guide 6: Interior Western United States, Geological Society of America, p. 27–52.

Shervais, J.W., Schmitt, D.R., Nielson, D., Evans, J.P., Christiansen, E.H., Morgan, L., Shanks, W.C.P., Prokopenko, A.A., Lachmar, T., Liberty, L.M., Blackwell, D.D.,

Glen, J.M., Champion, D., Potter, K.E., et al., 2013, First Results from HOTSPOT: The Snake River Plain Scientific Drilling Project, Idaho, U.S.A.: Scientific Drilling, doi: 10.2204/iodp.sd.15.06.2013.

Shervais, J.W., Shroff, G., Vetter, S.K., Matthews, S.H., Hanan, B.B., and McGee, J.J., 2002, Origin and Evolution of the Western Snake River Plain: Implications From Stratigraphy, Faulting, and the Geochemistry of Basalts Near Mountain Home, Idaho: Tectonic and Magmatic Evolution of the Snake River Plain Volcanic Province: Idaho Geological Survey Bulletin, v. 30, p. 343–361.

Shervais, J.W., and Vetter, S.K., 2009, High-K alkali basalts of the Western Snake River Plain (Idaho): Abrupt transition from tholeiitic to mildly alkaline plume-derived basalts: Journal of Volcanology and Geothermal Research, v. 188, p. 141–152, doi: 10.1016/j.jvolgeores.2009.01.023.

Shervais, J.W., Vetter, S.K., and Hanan, B.B., 2006, Layered mafic sill complex beneath the eastern Snake River Plain: Evidence from cyclic geochemical variations in basalt: Geology, v. 34, p. 365, doi: 10.1130/G22226.1.

Werner, R., and Schmincke, H.-U., 1999, Englacial vs lacustrine origin of volcanic table mountains: evidence from Iceland: Bulletin of Volcanology, v. 60, p. 335–354, doi: 10.1007/s004450050237.

Wheeler, H.E., and Cook, E.F., 1954, Structural and Stratigraphic Significance of the Snake River Capture, Idaho-Oregon: Journal of Geology, v. 62, p. 525–536.

White, C.M., Hart, W.K., Bonnichsen, B., and Matthews, D., 2002, Geochemical and Sr-isotopic variations in western Snake River Plain basalts, Idaho.: Tectonic and Magmatic Evolution of the Snake River Plain Volcanic Province. Idaho Geological Survey Bulletin 30, p. 329–342.

Wood, S.H., 1994, Seismic expression and geological significance of a lacustrine delta in Neogene deposits of the western Snake River Plain, Idaho.: AAPG Bulletin, v. 78, p. 102–121.

Wood, S.H., and Clemens, D.M., 2002, Geologic and tectonic history of the western Snake River Plain, Idaho and Oregon.: Tectonic and Magmatic Evolution of the Snake River Plain Volcanic Province: Idaho Geological Survey Bulletin, v. 30, p. 69–103.

Zhao, J., Brugger, J., Chen, G., Ngothai, Y., and Pring, A., 2014, Experimental study of the formation of chalcopyrite and bornite via the sulfidation of hematite: Mineral replacements with a large volume increase: American Mineralogist, v. 99, p. 343–354, doi: 10.2138/am.2014.4628.

APPENDICES

Appendix A

Description of core

Description	Depth (m bgs)
Massive gray basalt, some minor alteration.	165.2 – 171.6
Massive basalt with plagioclase phenocrysts. Laths form radial pattern.	171.6 – 184.4
Fractured massive basalt. Fractures filled with white colored secondary minerals.	184.4 – 194.2
Fractured massive basalt. Fractures filled with white colored secondary minerals. Dark colored, nearly black sections. Plagioclase phenocrysts present, laths form radial pattern.	194.2 – 200.0
Vesicular basalt, vesicles filled with white secondary minerals. Transitions into massive basalt with plagioclase phenocrysts.	200.0 – 203.6
Basalt sediments ranging in size from silt to coarse sand. Poorly sorted, some pebble sized clasts present.	203.6 – 214.6
Poorly sorted sandy silt.	214.6 – 415.7
Fine clay	415.7 – 435.9
Gravely sand. Medium to coarse-grained sand with abundant gravel.	435.9 – 441.1
Very fine, well sorted sand.	441.1 – 518.2
Basalt sand, poorly sorted, grains ranging in size from fine sand to gravel.	518.2 – 525.2
Basalt flow, vesicular to massive, rubbly at base.	525.2 – 527.0
Coarse basalt sand, poorly sorted	527.0 – 541.9
Fractured basalt, white fracture fill	541.9 – 544.4
Coarse sand	544.4 – 551.1
Lime mud, clay and silt	551.1 – 737.6
Basalt flow. Vesiculated basalt shows brown alteration of glassy rinds. Fractures filled with white secondary mineral.	737.6 – 752.9
Basalt sand	752.9 – 755.9
Basalt flow many fractures present, alteration of glasses, secondary minerals present throughout.	755.9 – 771.1
Dark brown mudstone, clay to silt.	771.1 – 858.6
Massive basalt, some alteration	858.6 – 862.0
Fractured mudstone, clay to silt	862.0 – 887.0

Highly altered basalt, individual flow termini indifferentiable. Many fractures present filled with white secondary minerals.	887.0 – 921.4
Basalt flow, vesicular to massive. Vesicles filled with white secondary minerals	921.4 – 923.2
Highly altered basalt, individual flow termini indifferentiable. Many fractures present filled with white secondary minerals.	923.2 – 933.9
Glassy basaltic breccia-like tuff-like section, low density. Faceted angular clasts millimeter to centimeter sized. Porous, and pores are filled with white secondary minerals.	933.9 – 996.1
Basalt sand, poorly sorted, clasts ranging in size from fine to coarse sand, with larger clasts floating, possibly debritic.	996.1 – 1003.7
Basalt flow, vesicular to massive. Vesicles filled with white secondary minerals	1003.7 – 1014.4
Basalt sand	1014.4 – 1026.6
Basalt flow, vesicular to massive. Vesicles filled with white secondary minerals	1026.6 – 1030.8
Basalt sand, poorly sorted, clasts ranging in size from fine to coarse sand, with larger clasts floating, possibly debritic.	1030.8 – 1034.8
Basalt flow, vesicular to massive. Vesicles filled with white secondary minerals	1034.8 – 1038.8
Basalt sand	1038.8 – 1042.4
Basalt flow, vesicular to massive. Vesicles filled with white secondary minerals. Some fractures, also filled with white minerals.	1042.4 – 1053.7
Basalt sand, poorly sorted, grains ranging in size from fine sand to gravel.	1053.7 – 1057.7
Basalt flow, vesicular to massive. Vesicles filled with white secondary minerals	1057.7 – 1069.2
Basalt sand, poorly sorted, clasts ranging in size from fine to coarse sand, with larger clasts floating, possibly debritic.	1069.2 – 1079.6
Basalt flow, vesicular to massive. Vesicles filled with white secondary minerals	1079.6 – 1093.6
Basalt sand, poorly sorted, clasts ranging in size from fine to coarse sand, with larger clasts floating, possibly debritic.	1093.6 – 1099.7
Basalt flow, vesicular to massive. Vesicles filled with white secondary minerals. Fractures present	1099.7 – 1103.4
Basalt sand, poorly sorted, grains ranging in size from fine sand to gravel.	1103.4 – 1104.9

Basalt flow, vesicular to massive. Vesicles filled with white secondary minerals	1104.9 – 1116.2
Highly altered basalt, individual flow termini indifferentiable. Many fractures present filled with white secondary minerals and pyrite.	1116.2 – 1143.9
Dark grey to black mudstone, clay to silt sized grains.	1143.9 – 1151.8
Glassy basaltic breccia-like tuff-like, low density. Faceted angular clasts millimeter to centimeter sized. Porous, and pores are filled with white secondary minerals.	1151.8 – 1164.0
Thick basalt flow vesicular to massive. Vesicles filled with white secondary minerals. Massive section has plagioclase phenocrysts. Brown and white secondary minerals in vein fill.	1164.0 – 1214.0
Basalt flow vesicular to massive. Vesicles filled with white secondary minerals.	1214.0 – 1220.1
Basalt sand, poorly sorted	1220.1 – 1222.6
Basalt flow vesicular to massive. Vesicles filled with white secondary minerals.	1222.6 – 1230.8
Basalt sand, poorly sorted, clasts ranging in size from fine to coarse sand, with larger clasts floating, possibly debritic.	1230.8 – 1236.6
Basalt flow vesicular to massive. Vesicles filled with white secondary minerals.	1236.6 – 1237.8
Basalt sand, poorly sorted, grains ranging in size from fine sand to gravel.	1237.8 – 1240.5
Basalt flow vesicular to massive. Vesicles filled with white secondary minerals.	1240.5 – 1244.5
Highly altered basalt, individual flow termini indifferentiable. Many fractures present filled with white secondary minerals, possibly clays present.	1244.5 – 1255.5
Basalt flow vesicular to massive. Vesicles filled with white secondary minerals. Glassy groundmass shows some clay alterations.	1255.5 – 1258.8
Basalt sand, poorly sorted	1258.8 – 1261.9
Basalt flows with a contact at	1261.9 – 1271.6
Glassy basaltic breccia-like tuff-like, low density. Faceted angular clasts millimeter to centimeter sized. Porous, and pores are filled with white secondary minerals.	1271.6 – 1276.8

A series of multiple basalt flows. Flow contacts are observed as both changes in flow facies and flow color, ranging from gray to nearly black. Plagioclase phenocrysts are observed in massive portions of the flows. Phenocrysts display a radial pattern in some cases.	1276.8 – 1331.4
Highly altered basalt, individual flow termini indifferentiable. Many fractures present filled with white secondary minerals, pyrite, possibly clays present.	1331.4 – 1343.3
Basalt flow, markedly less altered then the units above and below it.	1343.3 – 1347.2
Highly altered basalt. Many fractures present filled with white secondary minerals, pyrite, possibly clays present. Faults observed.	1347.2 – 1363.7
Brecciated unit, basalt fragments cemented by basalt clast matrix. White and brown secondary minerals present.	1363.7 – 1383.2
Highly altered basalt. Many fractures present filled with white secondary minerals, pyrite, possibly clays present. Large secondary crystals observed growing into open voids.	1383.2 – 1389.9
Basalt flow, markedly less altered then the units above and below it.	1389.9 – 1396.3
Highly altered basalt. Secondary minerals, pyrite, possibly clays present.	1396.3 – 1408.5
A series of multiple basalt flows. Flow contacts are observed as both changes in flow facies and flow color, ranging from gray to nearly black. Plagioclase phenocrysts are observed in massive portions of the flows. Phenocrysts display a radial pattern in some cases. Glassy matrix in massive sections degraded looking.	1408.5 – 1486.8
Brecciated unit, basalt fragments cemented by basalt clast matrix. White and brown secondary minerals present.	1486.8 – 1517.9
Highly altered basalt, individual flow termini indifferentiable. Many fractures present filled with white secondary minerals, pyrite, possibly clays present.	1517.9 – 1531.6
Massive basalt, mostly unaltered, some indication of degradation of glassy groundmass, observed as interstitial brown mineral. Two flow contacts observed as changes in flow facies from massive to vesicular.	1531.6 – 1708.1
Brecciated basalt	1708.1 – 1724.6
Zone of high alteration in basalt.	1724.6 – 1732.2
Basalt sand, fine grained and much lower density than units above and below.	1732.2 – 1737.4

Brecciated basalt. Angular basalt fragments in matrix of fine basalt clasts. Voids filled white minerals. Some large crystal growth observed in open void pockets.	1737.4 – 1749.6
Basalt flows. Flow contacts observed as changes in flow facies and/or color variations. Markedly less altered than units adjacent above and below.	1749.6 – 1795.3
Zone of relatively higher alteration. White secondary minerals abundant in pore space and fracture fill. Pyrite observed.	1795.3 – 1804.7
Basalt flow of lesser alteration. Vesicles filled with white secondary mineral. Interstitial glasses degraded in massive portion. Plagioclase phenocrysts in some massive units.	1804.7 – 1821.0

Appendix B

Sources for geographic information systems data layers

Blackwell, D.D., and Richards, M., 2004, Geothermal Map of North America: American Association of Petroleum Geologists.

- Heat flow

Dollison, R.M., 2010, The National Map: U.S. Geological Survey New viewer, services, and data download.

- Base maps
- Digital elevation map
- Surface faults
- Surface geology
- Geologic map scales

Duckworth, J., 2010, Geothermal Prospector: National Renewable Energy Laboratory.

- Cadastral maps

Heidbach, O., Tingay, M., Reinecker, J., Kurfe., D., and Müller, B., 2008, The World Stress Map database release:.

- Stress orientations

Lewis, R.S., Link, P.K., Stanford, L.R., and Long, S.K., 2012, Geologic Map of Idaho: Idaho Geological Survey Map-9 Web Map.

- Geothermal wells
- Ground water temperatures
- Major cities
- Major roads
- Oil and gas wells
- State border
- Thermal Springs
- Young fault

Lindholm, G.F., Garabedian, S.P., Newton, G.D., and Whitehead, R.L., 1987, Configuration of the water table and depth to water, spring 1980, water level fluctuations, and water movement in the Snake River Plain regional aquifer system, Idaho and eastern Oregon: U.S. Geological Survey Hydrologic Investigations Atlas.

- Groundwater aquifer thickness

Payne, S.J., McCaffrey, R., and King, R.W., 2008, Strain rates and contemporary deformation in the Snake River Plain and surrounding Basin and Range from GPS and seismicity: Geology, v. 36, p. 647, doi: 10.1130/G25039A.1.

- GPS vector data (strain rate)

Unpublished work by Shervais
- Vents by age
- Surface flow contacts in Mountain Home area